Comparative Proteomic Analysis Identifies Key Metabolic Regulators of Gemcitabine Resistance in Pancreatic Cancer

Authors

Qingxiang Lin, Shichen Shen, Zhicheng Qian, Sailee S. Rasam, Andrea Serratore, William J. Jusko, Eugene S. Kandel, Jun Qu, and Robert M. Straubinger

Correspondence

junqu@buffalo.edu; rms@buffalo.edu

Graphical Abstract

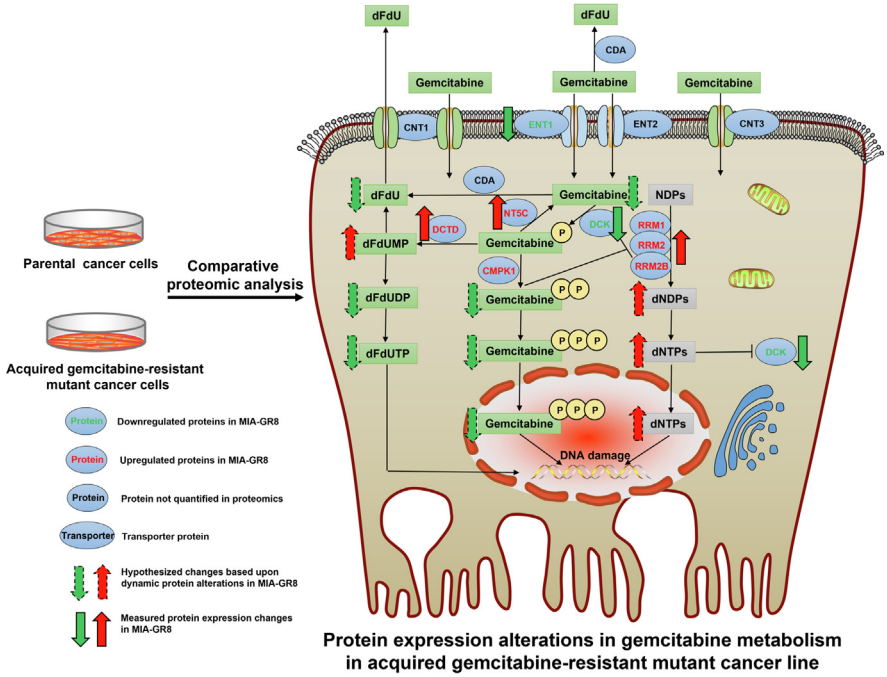

Protein expression alterations in gemcitabine metabolism in acquired gemcitabine-resistant mutant cancer line

In Brief

For pancreatic cancer (PDAC) patients, gemcitabine resistance (GemR) represents a major clinical problem. Global quantitative differential proteomic analysis of highly GemR PDAC cells developed from relatively Gem-sensitive PDAC cell lines identified multiple networks within the thousands of quantified proteins that support adaptation to Gem-induced stress, and reveal the complexity of GemR. Drug metabolism pathways were key contributors to GemR, and expression changes in Gem-metabolizing enzymes suggest both their influence upon Gem responsiveness, and drug-targetable vulnerabilities to improve clinical Gem efficacy.

Highlights

- Pancreatic adenocarcinoma cell lines 75× more resistant to gemcitabine (Gem) than parental cells were developed
- RRM1 and S100A4 were the most upregulated and downregulated proteins in GemR cells
- The predominantly altered GemR cell proteins were associated with cancer metabolism
- GemR cell alterations in Gem metabolism would reduce Gem activation/utilization
- Temporal responses to Gem suggested dynamic, adaptive drug resistance mechanisms

2022, Mol Cell Proteomics *21*(*10*), 100409

https://doi.org/10.1016/j.mcpro.2022.100409

Comparative Proteomic Analysis Identifies Key Metabolic Regulators of Gemcitabine Resistance in Pancreatic Cancer

Qingxiang Lin[1,2,3], Shichen Shen[2,3], Zhicheng Qian[2], Sailee S. Rasam[3,4], Andrea Serratore[2], William J. Jusko[2], Eugene S. Kandel[1], Jun Qu[1,2,3,4,*], and Robert M. Straubinger[1,2,3,5,*]

Pancreatic adenocarcinoma (PDAC) is highly refractory to treatment. Standard-of-care gemcitabine (Gem) provides only modest survival benefits, and development of Gem resistance (GemR) compromises its efficacy. Highly GemR clones of Gem-sensitive MIAPaCa-2 cells were developed to investigate the molecular mechanisms of GemR and implemented global quantitative differential proteomics analysis with a comprehensive, reproducible ion-current–based MS1 workflow to quantify ~6000 proteins in all samples. In GemR clone MIA-GR8, cellular metabolism, proliferation, migration, and 'drug response' mechanisms were the predominant biological processes altered, consistent with cell phenotypic alterations in cell cycle and motility. S100 calcium binding protein A4 was the most downregulated protein, as were proteins associated with glycolytic and oxidative energy production. Both responses would reduce tumor proliferation. Upregulation of mesenchymal markers was prominent, and cellular invasiveness increased. Key enzymes in Gem metabolism pathways were altered such that intracellular utilization of Gem would decrease. Ribonucleoside-diphosphate reductase large subunit was the most elevated Gem metabolizing protein, supporting its critical role in GemR. Lower Ribonucleoside-diphosphate reductase large subunit expression is associated with better clinical outcomes in PDAC, and its downregulation paralleled reduced MIAPaCa-2 proliferation and migration and increased Gem sensitivity. Temporal protein-level Gem responses of MIAPaCa-2 *versus* GemR cell lines (intrinsically GemR PANC-1 and acquired GemR MIA-GR8) implicate adaptive changes in cellular response systems for cell proliferation and drug transport and metabolism, which reduce cytotoxic Gem metabolites, in DNA repair, and additional responses, as key contributors to the complexity of GemR in PDAC. These findings additionally suggest targetable therapeutic vulnerabilities for GemR PDAC patients.

Pancreatic adenocarcinoma (PDAC) is the fourth leading cause of cancer death in the United States, with a median overall survival of 5.8 months and 5-years survival of 8% (1). It is projected to become the second most common cause of cancer death by 2040 (2). Because of advanced disease and metastases at diagnosis, approximately 85% of patients are not candidates for surgery, providing them limited treatment options. Gemcitabine (Gem) is standard-of-care but provides only a modest survival benefit (6.7 months; (3, 4)), because PDAC tumors are either intrinsically resistant to Gem or become Gem-resistant during therapy.

Gem resistance (GemR) arises from multiple factors. Dense desmoplastic stroma is a characteristic of PDAC and presents a physical barrier to drug delivery. The tumor microenvironment also promotes a drug-resistant phenotype (5–7). In addition, Gem exposure activates various survival pathways, including MAPK, NF-κB, heat shock proteins, fatty acid and sphingolipid metabolism, and pyruvate metabolism (8). Greater expression of downstream epithelial–mesenchymal transition (EMT) biomarkers, which is typically associated with metastatic phenotypes, correlates positively with GemR (9–12). Phenotypic and genetic adaptations can also reduce Gem cellular uptake and metabolism. Gem uptake utilizes several nucleoside transporters that impact tumor response, including the equilibrative nucleotide transporter 1 (ENT1, SLC29A1) (13). Increased ENT1 expression or activity is a predictive clinical marker for better Gem responses (14), underscoring its key role in modulating Gem sensitivity. Extracellular deamination of Gem by cytidine deaminase (CDA) transforms Gem into inactive difluorodeoxyuridine (dFdU), which is rapidly cleared (15). The dynamics of numerous nucleoside-related enzymatic systems control the concentrations of Gem metabolic products, thereby impacting Gem efficacy.

From the [1]Department of Cell Stress Biology, Roswell Park Comprehensive Cancer Center, Buffalo, New York, USA; [2]Department of Pharmaceutical Sciences, [3]Center of Excellence in Bioinformatics & Life Science, and [4]Department of Biochemistry, University at Buffalo, State University of New York, Buffalo, New York, USA; [5]Department of Pharmacology & Therapeutics, Roswell Park Comprehensive Cancer Center, Buffalo, New York, USA

*For correspondence: Jun Qu, junqu@buffalo.edu; Robert M. Straubinger, rms@buffalo.edu.

https://doi.org/10.1016/j.mcpro.2022.100409

Once taken up by cells, Gem is phosphorylated to its active diphosphate and triphosphate derivatives, including Gem diphosphate (dFdCDP) and Gem triphosphate (dFdCTP), by deoxycytidine kinase (DCK), the rate-limiting enzyme in intracellular Gem metabolism. During this process, 5′-nucleotidase (NT5C) and deoxycytidylate deaminase (DCTD) can inactivate Gem monophosphate (dFdCMP). Cytidine monophosphate kinase 1 (CMPK1) and nucleoside diphosphate kinase 1 (NDK1) sequentially convert Gem monophosphate into dFdCDP and dFdCTP. A molecular competition exists between dCTP and Gem metabolite dFdCTP as nucleotide sources for DNA synthesis. Ribonucleotide reductase (RNR) complex, consisting of ribonucleoside-diphosphate reductase large subunit (RRM1), ribonucleoside-diphosphate reductase subunit M2 (RRM2), and ribonucleotide-diphosphate reductase subunit M2 B (RRM2B), maintains the deoxyribonucleotide triphosphate (dNTP) pools (16). Upregulation of the RRM1 also contributes to GemR (17), and high RRM1 expression is associated with poor Gem responses in lung cancer patients (18, 19).

To maximize efficacy of Gem-based therapies and overcome GemR, additional agents such as nab-paclitaxel have been integrated empirically into the standard-of-care (4, 20). However, addition of nab-paclitaxel (Abraxane) to Gem increases median overall survival from 6.7 to 8.5 months (4). Thus, deciphering the molecular mechanisms of GemR is essential for developing more efficacious therapies for GemR PDAC.

Because alterations in the expression of effector protein systems modulate GemR, quantitative, differential proteomic analysis represents a powerful tool for investigating global, drug-mediated protein changes. Proteomic analysis holds significant advantages over transcriptomic analysis by circumventing the frequent nonconcordance between mRNA and protein expression. Previous studies employing comparative proteomic analysis to investigate GemR (21–25) were limited by the small numbers of proteins that 2D-DIGE/MALDI-TOF mass spectrometry could analyze (26). Here, we utilized global quantitative proteomic analysis to compare the differentially-expressed proteins in parental Gem-sensitive *versus* Gem-resistant cells. We employed *IonStar*, an MS1-based proteomics workflow that affords advantages over traditional MS1-based and label-based methods (27–29). It achieves excellent depth of coverage (6000–8000 proteins quantified in every sample), high quantitative accuracy without the cost of isobaric mass tags, an extremely low rate of missing data, and a stringent, low false-positive discovery rate (FDR) of significantly altered proteins (27). *IonStar* permits reproducible and well-controlled quantification of a large number of samples in a single batch, allowing temporal analysis of differential protein expression, and the ability of quantify small changes in protein abundance with high sensitivity and accuracy. We employed this proteomics workflow to investigate the global, proteome-level differences between Gem-sensitive and GemR PDAC cells, as well as their responses to Gem exposure, with a particular focus on protein changes in adaptive cellular response systems. This approach can provide insights into the production rate of cytotoxic Gem metabolites, inform as to additional cell response mechanisms to Gem treatment, and suggest strategies for the modulation of Gem metabolism to combat the resilience of this highly fatal cancer.

EXPERIMENTAL PROCEDURES

Reagents

Gem-HCl was purchased from LC Laboratories. Stock solutions of 1 mM were prepared in dimethyl sulfoxide (DMSO, Sigma-Aldrich) for *in vitro* assays and was dissolved in saline for *in vivo* studies.

Primary antibodies for the following proteins were obtained from the Cell Signaling Technology, and the working dilution used were RRM1 (#8637, 1:2000), Zeb1 (#3396, 1:1000), N-Cadherin (#13116, 1:600), Snail (#3879, 1:1000), Slug (#9585, 1:1000), Vimentin (#5741, 1:2000), cleaved-Caspase-3 (#9664, 1:800), and β-actin (#3700, 1:2000). Secondary anti-rabbit (#7074, 1:1000) and anti-mouse (#7076, 1:1000) antibodies were also obtained from Cell Signaling Technology.

Cell Lines and Cell Culture

The human PDAC cell lines MIAPaCa-2 and PANC-1 were purchased from American Type Culture Collection. All cells were cultured in Dulbecco's modified Eagle's medium (DMEM) (Cellgro) supplemented with 10% (v/v) fetal bovine serum (Cellgro; complete DMEM). Cell line identity was confirmed by short tandem repeat analysis at the Roswell Park Genomics Core.

Generation of GemR Cell Lines—GemR cell lines were derived from MIAPaCa-2 cells by continuous exposure to increasing concentrations of Gem for 9 months, starting at 50 nM and escalating once surviving cells grew for approximately a week. Single-cell clones were then selected, and escalation of the drug concentration was terminated when cell proliferation/survival dropped below <20 to 50%. Nine stable GemR clones were able to grow in 1 μM Gem (#1, #2, #3, #4, #8, #9, #18, #20, #21). GemR clone #8 (MIA-GR8) was able to grow in 3 μM Gem.

Cell Growth Inhibition Assay

Cells were seeded in 6-well plates at 1.5×10^5/well in 2 ml complete DMEM, and triplicate wells were exposed to various concentrations of Gem diluted from a stock in DMSO. Vehicle experimental controls contained DMSO at a concentration equal to the amount present in wells having the highest Gem concentration. After 3 days' exposure, attached cells were trypsinized, harvested, and counted using a Coulter Counter (Model Z2; Beckman Coulter). Each experimental group (control and treatment) was comprised of three biological replicates, and three technical replicates were performed.

Mathematical Modeling of Cell Responses to Gem Treatment

Concentration-response curves were obtained by cell counting for both MIAPaCa-2 and MIA-GR8 cells exposed to various concentrations of Gem for 72 h. The IC_{50} was determined by fitting the concentration–response data using the inhibitory Hill function:

$$R_d = R_{0\_d} \cdot \left(1 - \frac{I_{\max\_d} \cdot C_d^{\gamma d}}{IC_{50\_d}^{\gamma d} + c_d^{\gamma d}}\right)$$

where R_d is the total number of attached cells, R_{0_d} is cell number on Day 3 in the absence of drug exposure, I_{max_d} is the maximum

cell growth inhibition of Gem, IC_{50_d} is the concentration mediating half-maximal growth inhibitory effects of Gem exposure, γ_d is the Hill coefficient, and d refers to either MIAPaCa-2 or MIA-GR8 cells. ADAPT5 software (Biomedical Simulations Resource, University of South California, Los Angeles) was used for model fitting and parameter estimation. The computational code is provided Supporting Information and (17). Model fitting was analyzed using visual inspection of fitting, goodness-of-fit, the sum of squared residuals, the Akaike information criterion, and the coefficients of variance of the estimated parameters.

Cell Proliferation Assay

Cells were seeded in sextuplicate wells in 96-well plates at 2×10^3 cells/well and treated with a range of drug concentrations for 72 h. A modified MTS (dimethylthiazol tetrazolium salt) assay was used to evaluate cell proliferation (Aqueous One Solution; Promega). The MTS metabolite was quantified by absorption at 490 nm using a microplate spectrophotometer. Each experimental group (control and treatment) was comprised of six biological replicates, and three technical replicates were performed.

In Vitro *Migration Assay*

Cells (2×10^3) in serum-free medium containing vehicle or Gem were seeded in triplicate in the upper chambers of Transwell plates (Corning Life Sciences), and the lower wells contained complete medium with or without drugs. After 12 h, migrating cells in the upper chambers were fixed with 5% paraformaldehyde and stained with 0.1% crystal violet (Sigma-Aldrich), and the number of migrating cells was quantified manually from images (n = 9 fields per well) acquired using a microscope.

Western Blot Analysis

Cells were harvested using RIPA buffer containing Halt protease and phosphatase inhibitor cocktails (Thermo Scientific Inc) and vortexed multiple times on ice. The sample supernatant was collected after centrifuging (220*g* for 20 min, 4 °C), and the protein concentration was quantified by BCA assay. An equivalent amount of protein from each sample was loaded on 4 to 15% Tris-Bis gradient gels (Invitrogen) and transferred to PVDF membranes after electrophoretic separation. Membranes were blocked with 5% BSA (Fisher Scientific Inc) in PBS (Dulbecco's PBS) containing 0.1% Tween20. After incubation with the primary and secondary antibodies (*Reagents, above*), the luminescence signal from the membranes was acquired using an ECL substrate kit (Thermo Scientific) and scanned using a ChemiDoc MP gel imaging system (Bio-Rad).

Lentivirus-Based shRNA Knockdown Assay

The RNA interference reagents were obtained from the Genomics Shared Resource of Roswell Park Comprehensive Cancer Center.

The two anti-sequences targeting RRM1 were:

shRRM1#1: TGCTGTTGACAGTGAGCGCGGCCAAGTCAACATT GGATATTAGTGAAGCCAC AGATGTAATATCCAATGTTGACTTGGCCA TGCCTACTGCCTCGGA

shRRM1#2: TGCTGTTGACAGTGAGCGCGCAGATCTTTGAAACTA TTTATAGTGAAGCCACAGATGTATAAATAGTTTCAAAGATCTG CTT GCCTACTGCCTCGGA

The scrambled control sequence was:

TGCTGTTGACAGTGAGCGATCTCGCTTGGGCGAGAGTAAGTAGT GAAGCCACAGAT GTACTTACTCTCGCCCAAGCGAGAGTGCCTACT GCCTCGGA

The lentivirus packaging plasmids PMD2G and psPAX2 and lentivirus expression plasmid (pLKO.1) containing the RRM1 targeting sequence and a selectable puromycin resistance gene were mixed and transduced into HEK 293T cells using a LipoD293 transfection kit (Invitrogen) per the manufacturer's protocol. The culture medium was replaced with fresh medium 12 h after transfection. Forty-eight hours later, the lentivirus-containing medium was collected, filtered, and added to medium mixed with 10 μg/ml polybrene (Sigma-Aldrich). MIAPaCa-2 cells were incubated with the lentivirus for 24 h. One μg/ml puromycin (Sigma-Aldrich) was added after 48 h, and cells were incubated of 1 week to select for stable construct integration. Surviving cells were then amplified, and protein expression was evaluated using Western blots.

Cell Cycle Analysis

Cell samples suspended in PBS were fixed with 70% cold ethanol and stored at −20 °C for a maximum of 1 week. For analysis, the cells were collected by centrifugation (220*g* for 20 min at 4 °C), the supernatant was removed, and the cells were washed three times with staining buffer (BD Pharmingen). The cells were stained with propidium iodide–containing RNase (BD Pharmingen) for 30 min at room temperature and analyzed by flow cytometry (FACSCalibur; Becton Dickinson) to quantify DNA content based upon propidium iodide intensity. Cell cycle distribution data were analyzed using ModFit LT 4.0 software (Verity Software) to determine the fractions of the cells in G0/G1, S, and G2/M phases. Each experimental group (control and treatment) was comprised of three biological replicates, and two technical replicates were performed.

Seahorse Metabolic Assay

Oxygen consumption rate (OCR) and extracellular acidification rate (ECAR) were measured using an XF96 Extracellular Flux Analyzer (Seahorse Bioscience) (30). MIAPaCa-2 and MIA-GR8 cells were seeded in triplicate at 1.5×10^3 cells/well in XFe96 plates (Seahorse Bioscience), incubated for 24 h in a humidified, 37 °C incubator with 5% CO_2, washed three times with Seahorse assay media (Seahorse Bioscience) using the XF Prep Station, and incubated at 37 °C without CO_2 for 45 min prior to metabolic analysis. The mitochondrial stress test was performed in XF Base Medium containing 10 mM glucose, 1 mM sodium pyruvate, and 2 mM L-glutamine, and the following inhibitors were added at the final concentrations: oligomycin (2 μM), carbonyl cyanide 4-(trifluoromethoxy) phenylhydrazone (0.5 μM), and rotenone/antimycin A (0.5 μM each). The glycolytic stress test was performed in XF Base Medium containing L-glutamine (2 mM), glucose (10 mM), oligomycin (2 μM), and 2-deoxy-glycose (2-DG) (50 mM). After the Seahorse media were removed, cells were washed twice with PBS, lysed in RIPA buffer containing protease and phosphatase inhibitors as above, and the protein concentration was quantified by BCA assay to permit normalization of the OCR and ECAR values. Each experimental group (control and treatment) was comprised of three biological replicates, and two technical replicates were performed.

Sample Preparation for Mass Spectrometry

For comparative proteomic analysis, monolayer cultures of MIAPaCa-2 or MIA-GR8 cells at 90 to 100% cell confluency were resuspended, a sample was harvested (0 h), and then 10^6 cells were seeded in 10-cm dishes, with three biological replicates for each control and treatment group. A second set of triplicate samples were harvested at near-confluence, 96 h later. The samples taken at 0 h and 96 h were harvested using ACCUTASE (EMD Millipore), washed three times with cold PBS by centrifugation (220*g* for 20 min, 4 °C), suspended in RIPA lysis buffer containing protease and phosphatase inhibitors (as above), and stored at −80 °C until analysis using the *IonStar* proteomics workflow described previously (supplemental Fig. S2; (27, 28)). Two independent experiments (technical

replicates) were performed, resulting in two datasets (Dataset_1 and Dataset_2; see Data Availability, below).

For proteomic analysis of Gem treatment responses, triplicate monolayer cultures of PANC-1 cells (three biological replicates for each control and treatment group, one technical replicate) were treated with 20 nM Gem over 0 to 72 h (31). In a second experiment, triplicate MIAPaCa-2 and MIA-GR8 cells (three biological replicates for each control and treatment group for each cell line, two technical replicates) were exposed to Gem concentrations that were near-IC_{50} (7.5 nM), or high (1 μM) for 0 to 96 h. At defined intervals, the monolayer cells were trypsinized and combined with any detached cells in the culture supernatant by centrifugation (220*g* for 20 min, 4 °C). The cells were then washed by centrifugation (220*g* for 20 min, 4 °C) with cold PBS 3 times. The cell pellet was suspended in RIPA buffer containing protease and phosphatase inhibitors, followed by vortex mixing 3 times on ice. The cell lysates were then centrifuged (20,000*g* for 15 min, 4 °C), and the supernatant was collected. Protein concentrations were quantified by BCA assay, and the samples were then subjected to IonStar proteomic analysis (supplemental Fig. S2).

Surfactant-Aided Extraction, Precipitation, and On-Pellet Digestion

A surfactant-aided extraction/precipitation/on-pellet digestion (SEPOD) method was used for sample preparation (32). Pelleted cells were lysed in a cold buffered surfactant cocktail (RIPA lysis buffer containing cOmplete protease and PhosSTOP phosphatase inhibitors; Roche Applied Science), homogenized and sonicated on ice, and then clarified by centrifugation (20,000*g* at 4 °C for 30 min). Protein concentrations were quantified, and proteolytic digestion, reduction, and alkylation were carried out. Briefly, the denatured proteins were precipitated with cold acetone and collected by centrifugation. The protein pellets were rinsed with methanol, air-dried briefly, rehydrated, and digested with a proteomics-grade trypsin (Sigma-Aldrich), which specifically cleaves after K/R but not before P. The supernatants were then clarified by centrifugation and analyzed using the *IonStar* proteomics workflow (supplemental Fig. S2; (28, 29)).

Experimental Data Analysis

LC-MS raw files were searched against the Human Uniprot database (https://www.uniprot.org/proteomes, downloaded 11/03/2016) using the MS-GF+ search engine (version 10089, released July 16, 2013); 20,121 protein entries for the combined MIAPaCa-2 and MIA-R8 datasets or 20,371 for the PANC-1 dataset were searched (31). The search parameters included precursor ion mass tolerance of 20 ppm [Q Exactive (MS-GF+)], a maximum of two missed cleavages per peptide, and fixed modification of carbamidomethylation on cysteine and dynamic modifications of methionine oxidation and acetylation of N-terminal lysine. Peptide-spectrum match (PSM) filtering, protein inference/grouping, and global FDR control were accomplished using IDPicker (33). The PSM level FDR was controlled to 0.0295% using a Q-value threshold of 0.17%. The protein and peptide FDRs were controlled to <1% and <0.5%, respectively, with a required minimum of two unique peptides identified per protein. The filtered PSM list was generated by IonStarSPG.R, which is available at https://github.com/shichens1989.

Two mass spectrometry proteomics datasets are deposited at the ProteomeXchange Consortium *via* the PRIDE partner repository with the dataset identifiers PXD030861 (dataset of MIAPaCa-2 cell responses to Gem) and PXD030859 (dataset of MIA-R8 cell responses to Gem, with a comparative proteomic analysis of MIA-GR8 and MIAPaCa-2). Detailed information of protein identification (accession # in the Human Uniprot database, # of distinct peptides, and % coverage of each protein) and quantification is available in supplemental Tables S4, S5, S7, S8, S10 and S11. Peptide and protein identification information is provided in supplemental Tables S6, S9 and S12.

Experimental Design and Statistical Rationale for Mass Spectrometry Experiments

Appropriate sample sizes and control numbers for each proteomic experiment were determined by statistical power analysis and are described for each individual experimental component. The number of replicates acquired, including biological and technical replicates, and statistical methods used for analysis are described. Controls are all negative controls and consisted of cells that were exposed to drug-free media containing DMSO at a concentration that was equal to the highest concentration present in the drug-containing media. Results are shown as mean ± standard deviation. Two-sided student tests were performed, and p values <0.05 were considered statistically significant. The fold change in protein expression of MIA-GR8 cells at each time point was normalized to the expression of the same protein in parental MIAPaCa-2 cells at the same time point. Groups were compared using a two-sided, unpaired Student's t test. Relative ratios of protein expression exhibiting $\log_2$ fold change >0.5 and p values <0.05 were considered statistically significant. Comparison of survival curves for different treatment groups was performed using Kaplan–Meier analysis as implemented in Prism GraphPad v.8.

Reliability of Quantification Measurements

IonStar typically achieves 5~10% intragroup coefficients of variation between technical replicates of cell/tissue samples, and systematic variability was evaluated using an experimental null distribution (34). At least three biological replicates were included for control and treatment groups, and standard deviation was used to describe the variability among biological replicates. Groups were compared using a two-sided, unpaired student's t test. Relative ratios of protein expression exhibiting $\log_2$ fold change >0.5 and p values <0.05 were considered statistically significant.

Establishment of Tumors and in Vivo *Pharmacodynamic Responses to Gem*

All procedures involving animals were approved in advance by the Institutional Animal Care and Use Committees of the Roswell Park Comprehensive Cancer Center (Buffalo, NY) and the University at Buffalo, State University of New York.

Tumor Establishment and Propagation—MIAPaCa-2 tumors were established by *sc* injection of 5×10^6 MIAPaCa-2 cells in 1:1 serum-free DMEM:Matrigel (Corning Life Sciences) into the flank of C.B-Igh-1b/IcrTac-Prkdc^{scid} SCID mice obtained from a colony maintained at Roswell Park and housed under pathogen-free conditions. GemR MIA-GR8 tumors were established by *sc* injection of 10^7 MIA-GR8 cells in PBS. When MIA-GR8 tumors were palpable, the mice were administered increasing doses of Gem by *ip* injection twice weekly, escalating the Gem dose approximately every 2 weeks from 20 mg/kg to 40, 60, and 80 mg/kg/injection. When the tumors achieved a volume of 2000 mm^3, tumor fragments were passaged (below), and Gem selection was repeated. After four passages, viable MIA-GR8 tumors fragments were cryopreserved for further *in vivo* studies as described below.

Tumor Implantation—Tumors were harvested rapidly after euthanasia of donor animals, immersed in ice-cold RPMI-1640 (Cellgro), cut into $2 \times 2 \times 2$ mm^3 fragments under sterile conditions, and then implanted *sc* through a small incision in the abdominal skin of male SCID mice under isoflurane anesthesia.

Tumor Treatment and Measurement—When MIAPaCa-2 or MIA-GR8 tumor volumes reached 150 to 200 mm^3, mice were randomized into groups (n = 6/group) of equivalent mean volumes, and vehicle

(saline) or Gem was administered by *ip* injection at a dose of 30 or 60 mg/kg twice weekly for 3 weeks. Tumor volume was measured twice weekly using a caliper, and volume was calculated as (length × width^2 × 0.5). Body weight was measured twice weekly to monitor toxicity. Mice were removed from study when tumors reached a protocol volume limit of 2000 mm^3 or any dimension reached 20 mm.

Bioinformatic Functional Analysis

Gene Ontology (GO) annotation was conducted using DAVID (Database for Annotation, Visualization and Integrated Discovery) v6.8 (https://david.ncifcrf.gov/) (35) to provide functional annotations of differentially represented biological processes, cellular components, and molecular functions.

Patient Data Sources

De-identified data from PDAC patient tumors, stratified by protein expression levels, were obtained from The Human Genome Atlas (TCGA) database (https://www.cancer.gov/tcga) (36) and processed using the online resource LOGpc (http://bioinfo.henu.edu.cn/DatabaseList.jsp) (37, 38). Transcriptomics data for PDAC patient tumors (n = 176 patient tumors) were also obtained from TCGA. Normalized FPKMs (fragments per kilobase of exon per million reads) were used to quantify the expression of each gene, with a detection threshold of 1 FPKM. The values of FPKM from TCGA were then converted into transcripts per million for comparing tissue expression data extracted from different databases. The transcriptomics data for normal pancreatic tissues (n = 247 individuals) were obtained from the genotype-tissue expression (GTEx) database (https://www.gtexportal.org/) (39–41).

RESULTS

Comparative Responses of MIAPaCa-2 and Gem-Resistant MIA-GR8 Cells to Gem

To gain insight into the molecular mechanisms of GemR, a panel of GemR cell lines was generated from parental MIAPaCa-2 cells by continuous *in vitro* exposure to escalating Gem concentrations (supplemental Fig. S1*A*). Figure 1 shows the effect of Gem upon cell proliferation for both the parental and GemR cells. The IC_{50} of Gem was 8.29 nM for parental MIAPaCa-2, and 627.29 nM for the highly GemR MIA-GR8 line, an increase of nearly 100-fold compared to the parental line (Fig. 1, *A* and *B*). Parameter estimates are shown in Table 1. Whereas 50 nM Gem inhibited proliferation of MIAPaCa-2 cells by 95% (I_{max_MIA} = 0.95), it showed negligible effect upon MIA-GR8 cells. A 200-fold higher concentration of Gem (10 μM) suppressed MIA-GR8 cell proliferation to only 82% of maximal (I_{max_GR8} = 0.82). In the absence of Gem, MIA-GR8 cells appeared spindle-shaped compared to MIAPaCa-2 cells (Fig. 1*C*), suggesting that MIA-GR8 had acquired

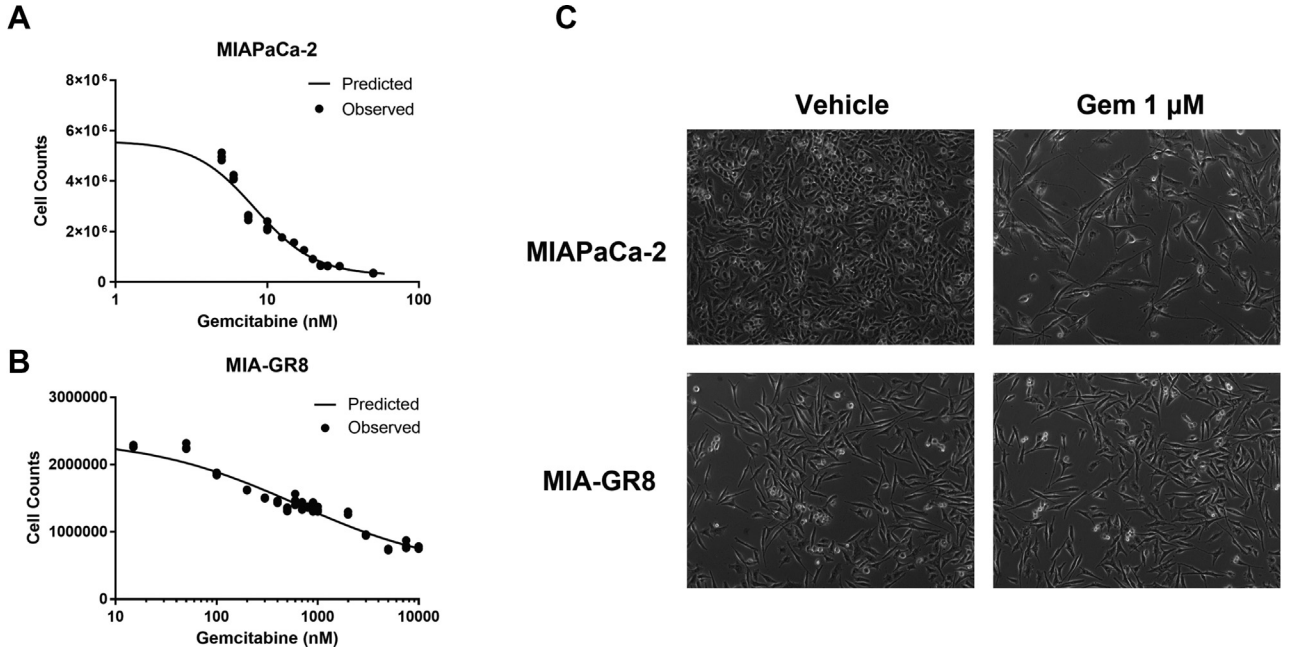

FIG. 1. **Development and characterization of MIAPaCa-2-derived GemR MIA-GR8 cell line.** GemR cell lines were derived from MIAPaCa-2 PDAC cells by continuous, escalating Gem exposure. *A*, concentration/cell proliferation response curves for parental MIAPaCa-2 cells; *B*, the highly GemR MIA-GR8 cell line over 72 h of exposure to the indicated Gem concentrations. *Symbols* denote observed cell counts, and *dotted lines* represent fitted curves using the inhibitory Hill function. Drug-specific parameters for both cell lines were estimated by simultaneous fitting of all data using ADAPT5 software and are provided in Table 1. *C*, morphology of MIAPaCa-2 and MIA-GR8 cells in the absence or presence of 1 μM Gem. Cells were exposed to vehicle or drug for 24 h, washed with PBS, fixed with paraformaldehyde, and imaged by phase-contrast microscopy. After 24 h of Gem exposure, parental MIAPaCa-2 cells had a more apoptotic appearance and grew slowly, whereas MIA-GR8 cells remained spindle-shaped and grew without obvious drug-mediated delay. Gem, gemcitabine; GemR, gemcitabine resistance; PDAC, pancreatic adenocarcinoma.

TABLE 1
Model parameter estimation for Gem IC_{50} on MIAPaCa-2 and MIA-GR8 cells

Parameter (units)	Definition	MIAPaCa-2		MIA-GR8	
		Estimate	CV%	Estimate	CV%
R_0 (1×10^6 cells)	Final cell counts in vehicle group	5.56	6.5	2.23	3.9
I_{max}	Maximal inhibitory effect of Gem	0.954	0.9	0.820	8.5
IC_{50} (nM)	Gem concentration mediating half-maximal growth inhibition	8.29	7.3	627	26.8
γ	Hill coefficient for Gem	2.18	7.5	0.580	17.0

an enhanced mesenchymal phenotype or stemness state (9, 11, 42) that is associated with drug resistance. MIAPaCa-2 cells became more spindle-shaped and apoptotic with 24 h of exposure to 1 μM Gem, but MIA-GR8 morphology did not change further (Fig. 1*C*).

Cell Cycle Distribution Analysis of MIAPaCa-2 Cells and MIA-GR8 Cells

Untreated MIA-GR8 cells grew much more slowly than MIAPaCa-2 cells (Fig. 2*A*), likely an adaption to cytotoxic agents that inhibit cell proliferation. Cell cycle progression, evaluated by flow cytometry, showed nearly 60% of MIA-GR8 cells were in the quiescent, nonproliferative G_0 phase or in G_1 phase, whereas less than 40% of MIAPaCa-2 cells were in G_0/G_1 phase (Fig. 2, *B* and *C*), and twice as many cells were in S phase compared to MIA-GR8 cells.

Increased EMT and Invasiveness of MIAPaCa-2 GemR Cells

EMT contributes to GemR (43). A hallmark of EMT is increased migration and invasiveness (10), and increased expression of mesenchymal markers such as Zeb1 and Slug. Compared to their expression in parental MIAPaCa-2 cells, Zeb1 and Slug were elevated in the majority of the nine GemR cell lines generated (Fig. 2*D*). In MIA-GR8, the most GemR cell line, cell motility also increased compared to parental MIAPaCa-2 cells (Fig. 2*E*).

Differential Responses of MIAPaCa-2 and MIA-GR8 Tumors to Gem Treatment

To investigate the persistence and impact of the GemR phenotype of MIA-GR8 cells, parental and GemR cells were implanted in SCID mice, and when tumors were palpable, mice were treated with escalating Gem doses over four passages to ensure *in vivo* selection of the GemR phenotype (supplemental Fig. S1*B*). In a subsequent passage, the effect of Gem on tumor volume progression was compared for MIAPaCa-2 and MIA-GR8 tumors. Without treatment, MIA-GR8 tumors grew more slowly than did MIAPaCa-2 tumors (Fig. 3, *A* and *C*), consistent with the observed differences in their relative *in vitro* cell proliferation rates. Over three cycles of twice-weekly treatment with 30 mg/kg Gem, MIAPaCa-2 tumor volume progression decreased significantly compared to controls ($p < 0.05$; Fig. 3*A*), and the median time of tumor progression to a threshold of 2000 mm^3 was also delayed significantly ($p < 0.05$; Fig. 3*B*). In contrast, neither the same treatment regimen nor doubling the Gem dose to 60 mg/kg had a significant effect upon MIA-GR8 tumor progression (Fig. 3, *C* and *D*), confirming the stability of its GemR phenotype *in vivo*.

Quantitative Differential Proteomic Analysis of MIAPaCa-2 and MIA-GR8 Cell Lines

Global differential protein expression analysis was performed using the *IonStar* proteomic analysis workflow (supplemental Fig. S2) on nearly confluent MIAPaCa-2 and MIA-GR8 cells at either the time of subculturing (day 0) or after 4 days of growth. *IonStar* combines carefully optimized experimental procedures for sample preparation with in-depth, reproducible, and well-controlled LC/MS analysis, and a pipeline for proteomic data analysis that achieves very low missing data, a quantifiable and low FDR, and superior accuracy and precision (27–29). Comparison of cells harvested at near confluence (~90–95%) on day 0 with nearly confluent cells harvested after 4 days of culture enabled us to investigate protein expression patterns in cells that had grown to similar cell densities. Two independent experiments were performed, yielding Dataset_1 and Dataset_2. Proteins were quantified using stringent criteria (FDR <1%; FDR for quantified peptides <0.1%, with at least two quantified peptides per protein). Dataset_1 contained 5993 proteins and Dataset_2 contained 5514 proteins (supplemental Fig. S3*A* and supplemental Tables S4–S12). The two datasets quantified 5128 proteins in common, suggesting excellent quantitative reproducibility across two independent experiments. Dataset_1 was investigated in greater detail because it contained more quantified proteins than Dataset_2.

For confident identification of differentially expressed proteins, fold change in protein expression between MIA-GR8 and MIAPaCa-2 cells was analyzed using an experimental null method that allows estimation of the FDR arising from technical variability (34). Using this method, the optimal cutoff selected was fold change ≤ 0.75 or ≥ 1.4 with $p \leq 0.05$, and 505 proteins were differentially expressed on both days (Fig. 4*A*). On day 0, 411 proteins were upregulated significantly in MIA-GR8 cells compared to the parental cell line, 496

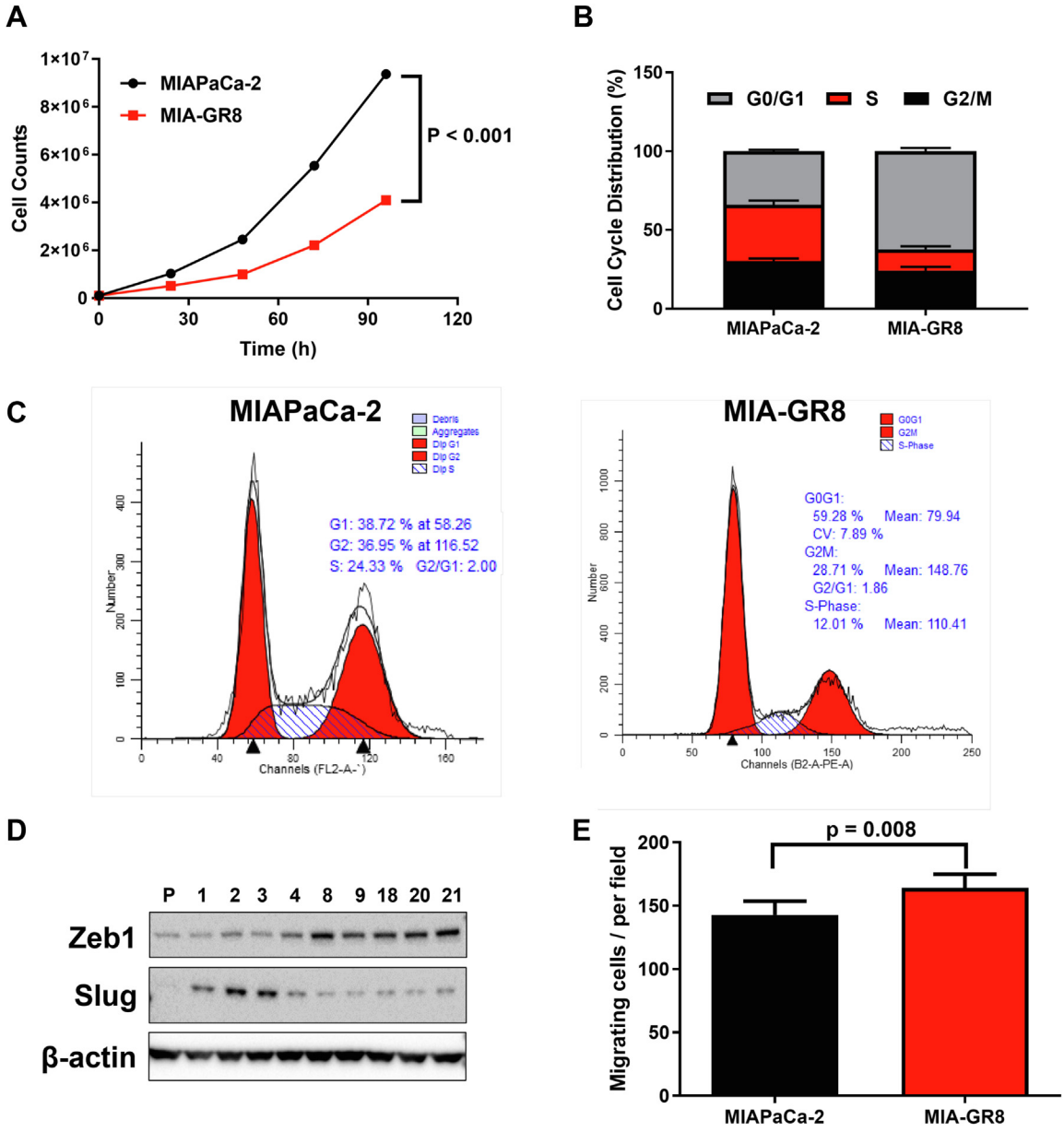

FIG. 2. **Proliferation, migration, and protein expression of parental MIAPaCa-2 cells and derived GemR MIA-GR8.** *A*, comparison of unperturbed growth rates of MIAPaCa-2 and MIA-GR8 cells over 96 h. Cells were detached at intervals and counted using a Coulter counter. *B*, comparison of cell cycle distribution (G_0/G_1, S, and G_2/M phases) of MIAPaCa-2 *versus* (*C*) MIA-GR8 cells during exponential growth, based on flow cytometry quantification of propidium iodide DNA staining. The fractions in each cell cycle phase were analyzed using Modfit software. *D*, Western blot showing comparative expression of mesenchymal markers in parental ("P") MIAPaCa-2 cells and nine stable GemR clones (listed above the lanes) derived from MIAPaCa-2 cells. *E*, comparison of MIAPaCa-2 and MIA-GR8 cell migration. A Transwell assay was used to determine the number of migrating MIAPaCa-2 and MIA-GR8 cells per field over 12 h. At the end of the incubation period, nonmigrating cells in the upper chamber were removed with cotton swabs. Migrating cells in the lower chamber were washed, fixed with 5% paraformaldehyde, stained with crystal violet, and imaged with a 40 × microscope objective, and migrating cells per image field were enumerated manually. Data are shown as mean ± SD. Gem, gemcitabine; GemR, gemcitabine resistance.

proteins were upregulated on day 4, and 223 shared proteins were upregulated in both cultures (Fig. 4*B*). On day 0, 510 proteins were downregulated significantly in MIA-GR8 cells relative to MIAPaCa-2 cells, 773 proteins were downregulated on day 4, and 265 shared proteins were downregulated on both days (Fig. 4*C*). Thus, differential proteomic analysis produced a rich dataset identifying a comparatively large number of quantified proteins that were constitutively altered in expression by the long-term, escalating Gem exposure that produced the highly GemR MIA-GR8 cell line.

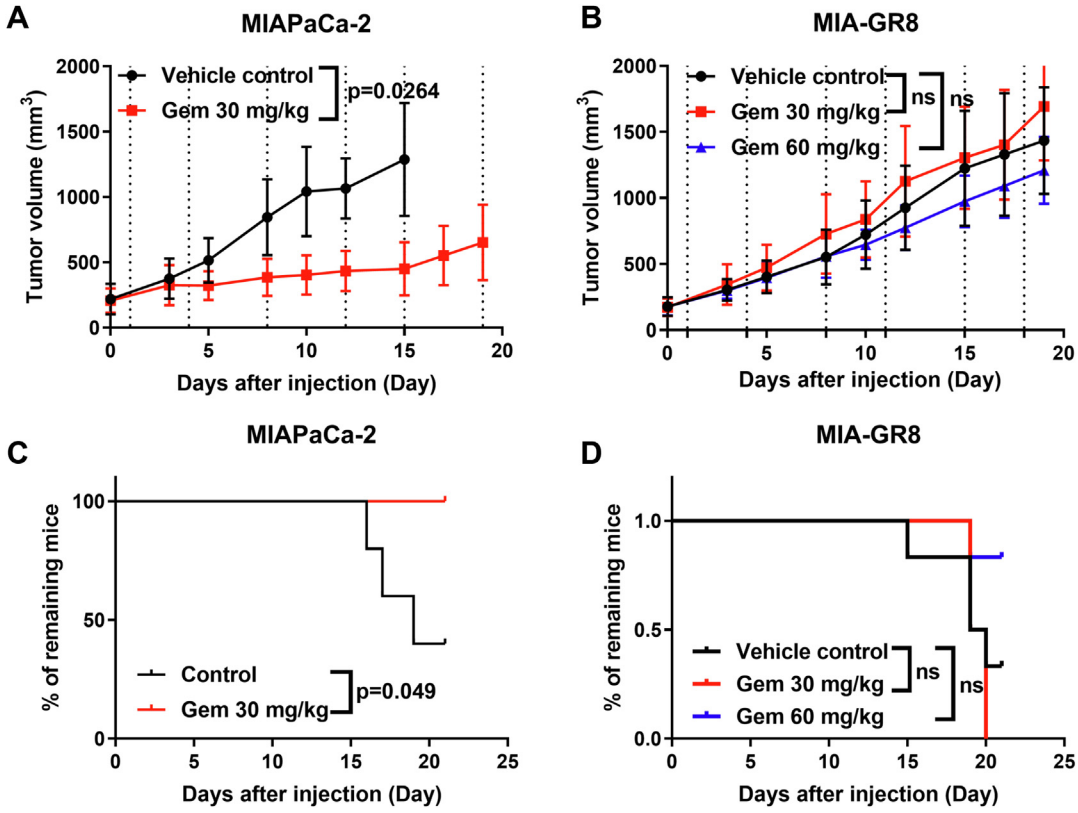

FIG. 3. **Gemcitabine efficacy on MIAPaCa-2 and MIA-GR8 xenografts.** *A*, *in vivo* growth rate of MIAPaCa-2 in the absence or presence of Gem treatment. *B*, *in vivo* growth rate of MIA-GR8 tumors (n = 6 mice/group) in the absence or presence of Gem treatment. When tumor volumes reached 150 to 200 mm^3, mice were randomized and administered saline or Gem (30 or 60 mg/kg *ip*) twice weekly for 3 weeks. *Vertical dashed lines* indicate treatment days. Tumor volumes and body weight were recorded over 3 weeks. Mice were removed from study when tumors reached a volume of 2000 mm^3 or any dimension reached 20 mm. When the second animal from any group was removed from study, data are no longer plotted to avoid bias of the mean. Gem treatment inhibited MIAPaCa-2 tumor growth significantly ($p < 0.05$) by day 15, but not the growth of MIA-GR8 tumors ($p > 0.05$). *C*, time of tumor progression to a threshold tumor volume of 2000 mm^3. Gem treatment delayed median time of MIAPaCa-2 tumor progression significantly ($p < 0.001$) compared with controls, but (*D*) MIA-GR8 tumor progression was not altered significantly by treatment ($p > 0.05$). Data shown are mean ± SD; ns: not significant ($p > 0.05$). Gem, gemcitabine.

GO Analysis of Differentially Expressed Proteins in GemR Cells

GO analysis of the differentially expressed proteins in MIA-GR8 cells indicated that the predominant drug-adaptive biological processes in these highly GemR cells include energy generation/utilization, cell division and proliferation, migration, and 'drug response' mechanisms, including DNA repair mechanisms and resistance to apoptosis (Fig. 5*A* and supplemental Table S1). The highest number of proteins altered in MIA-GR8 cells participate in oxidation–reduction processes (19.4% of the 592 proteins comprising this ontology category), including processes associated with the kinetics of energy balance and drug metabolism. Notably, proteins in Gem metabolism pathways appear in this category, including RRM1, RRM2, RRM2B, NT5C, and CMPK1 (16), suggesting that the capability for intracellular accumulation of active Gem in GemR cells was decreased as a response mechanism to Gem-induced stress. The biological processes associated with cell proliferation that were altered in MIA-GR8 cells include cell division (73/350 proteins, 20.9% of constituent proteins in category), mitotic nuclear division (51/248, 20.6%), DNA replication (29/155, 18.7%), and cell cycle (30/217, 13.8%) (Fig. 5*A*). Biological processes associated with cell movement enriched in MIA-GR8 cells include cell–cell adhesion (61/271, 22.5%), regulation of cell shape (29/140, 20.7%), cell migration (28/172, 16.3%), and small GTPases (31/246, 12.6%). This multiplicity of changes represents the diverse mechanistic responses driving GemR cells as they underwent EMT, which facilitates cell invasion and drug resistance. In parallel, proteins comprising 'drug response mechanisms' were altered significantly in MIA-GR8 cells; the data suggest that these GemR cells developed adaptations such as modified DNA repair (37/235), vesicular transport (51/395), and apoptosis resistance (59/455) in order to avoid Gem-induced responses such as apoptosis. Overall, the spectrum of MIA-GR8 cell responses to Gem-induced stress suggest

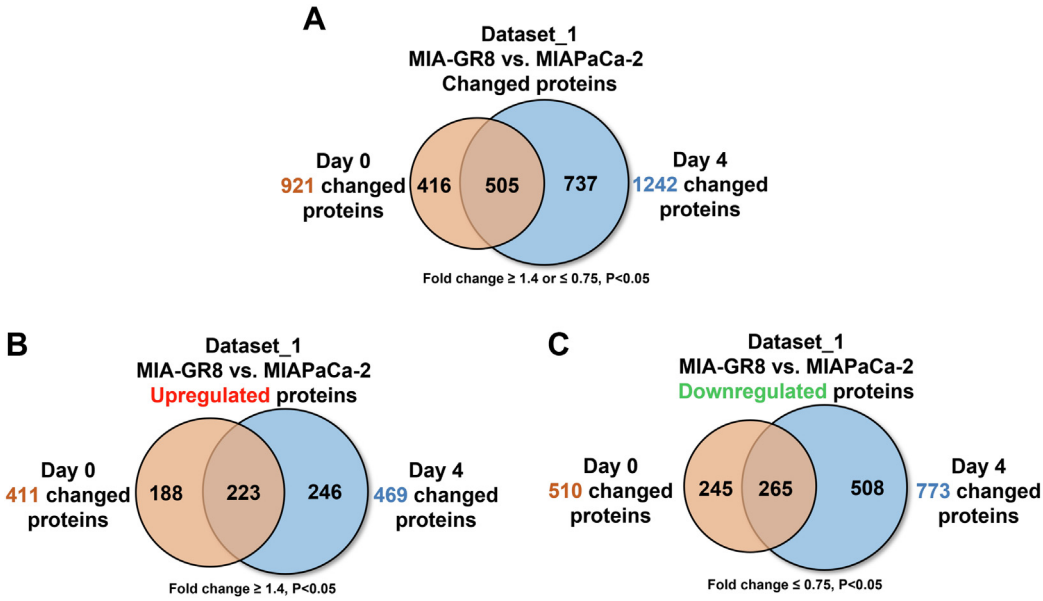

FIG. 4. **Comparative proteomic analysis of significantly changed proteins quantified in MIAPaCa-2 and MIA-GR8 cells.** Differential proteomics Dataset_1 consists of 5993 proteins quantified from both MIAPaCa-2 and GemR MIA-GR8 cells sampled at two time points (days 0 and 4 of culture), with no missing data, using the *IonStar* differential proteomic analysis workflow. *A*, a total of 1693 quantified proteins were differentially expressed in MIA-GR8 cells *versus* MIAPaCa-2 cells on days 0 and 4 of culture, with upregulation defined as ≥1.4-fold change and downregulation as ≤0.75-fold change) at $p < 0.05$; *B*, upregulated proteins in MIA-GR8 cells; *C*, downregulated proteins in MIA-GR8 cells. The number of shared proteins that were similarly regulated on days 0 and 4 are shown in the intersection of the *two circles*. Gem, gemcitabine; GemR, gemcitabine resistance.

that its GemR phenotype is both broadly based and attained through a range of mechanisms.

Adaptations in Energy Production in GemR Cells

Both differential proteomic analysis and the slower proliferation rate of MIA-GR8 cells *in vitro* and *in vivo* suggested that alterations energy generation/utilization developed as an adaptive response to Gem-induced stress in MIA-GR8 cells. To test this hypothesis, the kinetics of cell metabolism, glycolysis, and mitochondrial respiration were investigated. Compared to parental MIAPaCa-2 cells, MIA-GR8 cells had a lower ECAR (Fig. 5, *B* and *C*), suggesting a lower glycolytic capacity, reserve, and level of glycolysis. In addition, MIA-GR8 cells showed a lower OCR, based upon several measures of mitochondrial function that include basal mitochondrial respiration, proton leakage, maximal respiration rate, spare respiratory capacity, nonmitochondrial oxygen consumption, and ATP production (Fig. 5, *D* and *E*). Thus, these GemR cells developed a mechanism of reduced energy production in parallel with a reduced proliferation rate to reduce the impact of stress created by cytotoxic agents that predominantly target rapid cell growth.

Characterization of Significantly Enriched Proteins in GemR Cells

A more stringent cutoff was applied to the dataset in order to focus upon the subset of proteins differentially expressed between MIA-GR8 cells and parental MIAPaCa-2 cells that were the most consistently altered and greatest in magnitude: $\log_2$ fold change >2 or <–2 (fold change >4 or <1/4), and $-\log_{10}$ *p* value >2 ($p < 0.01$; Fig. 5, *F* and *G*). Among the upregulated proteins in this subset, RRM1 had the highest fold change (23.6- and 20.4-fold day 0 and day 4 samples of nearly confluent cells) and the lowest *p* values (8.1E-8 and 5.3E-8 for the day 0, day 4 samples). Additional upregulated proteins were characterized ontologically as modulating resistance to chemotherapy and radiation (Table 2). A role of these proteins in GemR has not been described previously.

Among the highly downregulated proteins, S100A4 (S100 calcium binding protein A4) had the greatest fold change in MIA-GR8 cells (0.07- and 0.3-fold for the day 0, day 4 samples) and lowest *p* values (8.97E-6 and 2.0E-6 for the day 0, day 4 samples). S100A4 has been reported as a driver of tumor progression and metastasis in various malignant tumors, including PDAC (44), and as a candidate biomarker for early diagnosis or prediction of cancer metastasis (45, 46), although numerous factors, including cancer type and drug class, may affect its role in drug resistance.

Surprisingly, a number of proteins that were downregulated in MIA-GR8 cells have been reported to promote drug resistance in other cancer types (Table 2). It is possible that these proteins contribute to GemR in PDAC in different ways, in that other chemoresistance mechanisms may override the contribution of the response networks represented by these proteins.

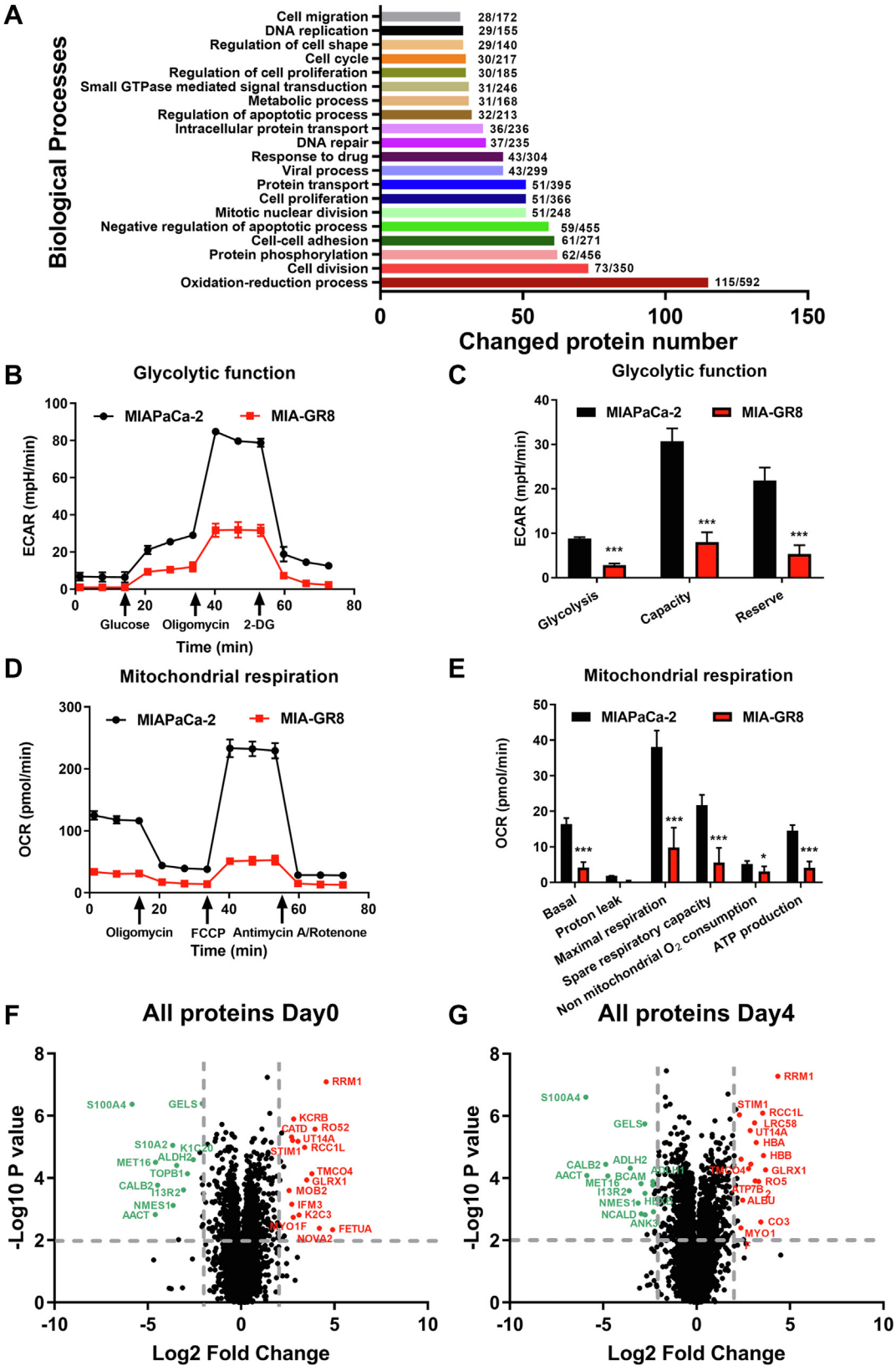

FIG. 5. **Ontology analysis of enriched proteins in GemR MIA-GR8 cells.** *A*, top biological processes enriched significantly in the GemR MIA-GR8 cell line, based upon a global differential expression proteomics workflow (Experimental Procedures). Results were analyzed using the

TABLE 2
Additional differential proteins associated with drug resistance in the comparative proteomic analysis

Proteins	Fold change at 0 h (*p* value)	Fold change at 96 h (*p* value)	References
FETUA (AHSG, alpha 2-HS glycoprotein)	29.9 (4.0E-3)	22.7 (0.03)	(78)
KCRB (CKB, creatine kinase B)	7.1 (1.3E-6)	6.9 (5E-5)	(87)
RO52 (TRIM21, tripartite motif containing 21)	15.6 (2.7E-6)	10.1 (1.3E-4)	(88, 89)
CATD (CTSD, cathepsin D)	6.5 (4.8E-6)	4.3 (6.2E-7)	(88, 90–93)
STIM1 (stromal interaction molecule 1)	6.8 (6.2E-6)	4.9 (9.1E-7)	(90–95)
ATP7B (ATPase copper transporting beta)	3.5 (1.8E-3)	8.8 (1.2E-4)	(94–102)
S100A4 (S100 calcium binding protein A4)	−0.01 (4.3E-7)	−0.01 (2.5E-7)	(73, 96–102)
ADLH2 (aldehyde dehydrogenase 2 family member)	−0.09 (3.9E-5)	−0.09 (4.8E-5)	(73, 103–106)
GEL2 (GSN, gelsolin)	−0.24 (4.1E-7)	−0.15 (1.8E-6)	(103–108)
CALB (calbindin 2)	−0.04 (1.7E-4)	−0.03 (3.6E-5)	(107–110)
AACT (SERPINA3, serpin family A member 3)	−0.04 (1.5E-3)	−0.02 (8.2E-5)	(109–111)

Contribution of RRM1 to GemR

Differential proteomic analysis identified RRM1 as the most significantly upregulated protein in MIA-GR8 cells (Fig. 5, *C* and *D*), a phenotypic change that was observed in all nine GemR clones developed from parental MIAPaCa-2 cells (Fig. 6, *A* and *C*), suggesting a significant role of RRM1 in modulating GemR in these clones. In the highly GemR MIA-GR8 cells, RRM2 was also upregulated (Fig. 6*B*), implicating both RRM1 and RRM2 as contributors to GemR in PDAC.

In other contexts, RRM1 has been considered a tumor suppressor (47), and in transgenic mouse models of lung and colon cancer, RRM1 overexpression was reported to decrease cancer metastases and extend survival (48–50). To provide further insight into the role of RRM1 in PDAC, MIA-PaCa-2 cells were transduced with specific shRNAs against RRM1, which would create an imbalanced pool of dNTPs. Knockdown of RRM1 by shRNA decreased cell viability by upregulation of apoptosis mediator–cleaved caspase 3 (Fig. 6, *D* and *E*), suggesting a key role of RRM1 to sustain the pool of dNTPs required for cancer proliferation. Consistent with a previous study (51), downregulation of RRM1 expression enhanced Gem inhibition of MIAPaCa-2 cell proliferation (Fig. 6*F*). RRM1-deficient cells also exhibited reduced migration in a Transwell assay and decreased expression of mesenchymal biomarkers Zeb1 and N-cadherin (Fig. 6*D*), indicating a reduction or reversal of the EMT phenotype.

Based upon these findings, we examined the association of RRM1 expression with clinical outcomes in PDAC patients using the LOGpc database (http://bioinfo.henu.edu.cn/DatabaseList.jsp) (37). RRM1 was more highly expressed in patient pancreatic cancers than in their normal pancreas tissues (Fig. 6*I*) based on TCGA (https://www.cancer.gov/tcga) and GTEx (https://www.gtexportal.org/) databases, suggesting potential clinical benefit of targeting RRM1 by combining Gem with other RNR complex inhibitors such as hydroxyurea. Kaplan–Meier survival plots also showed a significant inverse correlation between expression of RRM1 and PDAC patient survival (Fig. 6*J*), further supporting the role of RRM1 in PDAC progression and treatment resistance.

Adaptations in Gem Metabolism Supporting GemR

KEGG analysis of the differentially expressed proteins in MIA-GR8 cells showed that the greatest number of significantly changed proteins belongs to the metabolic pathway category (supplemental Fig. S3*C*), which includes most of the key enzymes in Gem metabolism that were quantified here, such as RRM1, RRM2, RRM2B, NT5C, thymidylate synthetase (TYMS), and CMPK1. These adaptations of MIA-GR8

David database (https://david.ncifcrf.gov/). Compared with parental MIAPaCa-2 cells, the predominant altered proteins in GemR cells include cell proliferation, migration, energy generation/utilization, and 'drug response' mechanisms. Numbers beside each column indicate the number of enriched proteins in each category relative to the number of proteins in the category. *B*, validation of drug-resistance mechanisms suggested by differential proteomic analysis. Glycolytic functions of MIAPaCa-2 and MIA-GR8 cells were compared using an Agilent Seahorse XF Glycolysis stress test. Glucose, oligomycin, and 2-deoxyglucose were introduced into the system at times marked by *arrows*. The extracellular acidification rate was measured to assess (*C*) key parameters including glycolysis, glycolytic capability, and glycolytic reserve. *D* and *E*, comparison of mitochondrial respiration functions. *D*, oligomycin, FCCP, and a mixture of antimycin A + rotenone were introduced into the system at times marked by *arrows*. The oxygen consumption rate was measured to assess (*E*) key characteristics including basal respiration, proton leak, maximal respiration, spare respiratory capacity, mitochondrial oxygen consumption, and ATP production. *F*, volcano plots of fold expression change for all quantified of protein in MIA-GR8 *versus* MIAPaCa-2 cells at 0 h and (*G*) 96 h of culture. *Green circles* indicate downregulated proteins, and *red circles* indicate upregulated proteins. *Gray dashed lines* indicate a more stringent fold change cutoff (fold change ≤0.25-fold (*left*) or ≥4-fold (*right*) at $p < 0.01$). Data are shown as mean ± SD. * $p < 0.05$, ** $p < 0.01$, *** $p < 0.001$. 2DG, 2-deoxyglucose; ECAR, extracellular acidification rate; FCCP, carbonyl cyanide 4-(trifluoromethoxy) phenylhydrazone; Gem, gemcitabine; GemR, gemcitabine resistance; OCR, oxygen consumption rate.

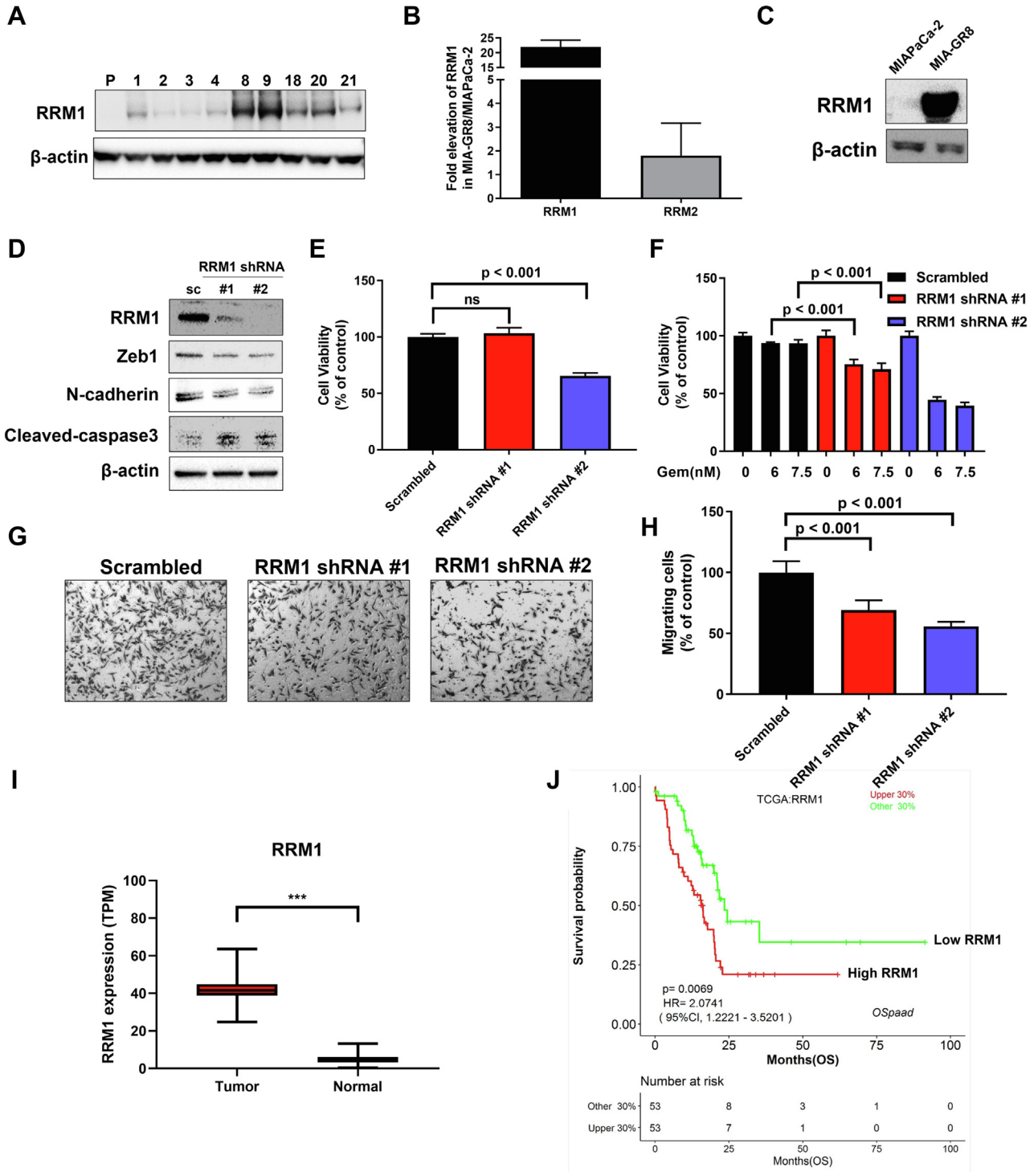

FIG. 6. **Effects of RRM1 on PDAC cell proliferation, migration, and Gem sensitivity.** *A*, Western blot analysis of RRM1 expression among parental MIAPaCa-2 cells (P) and nine stable GemR clones (listed above plot). *B*, quantification of fold change in expression of RRM1 and RRM2 in MIAPaCa-2 and MIA-GR8 cells based upon differential proteomic analysis (Experimental Procedures). *C*, Western blot confirmation of RRM1 expression in the MIAPaCa-2 and MIA-GR8 cell samples evaluated by differential proteomic analysis. *D*, confirmation of RRM1 knockdown in MIAPaCa-2 cells. Cells were stably transduced with nonsilencing shRNA (scrambled) or two specific shRNAs against RRM1 (RRM1 shRNA #1, #2). Western blot analysis shows downregulation of proteins associated with mesenchymal phenotypes (Zeb1 and N-cadherin) and upregulation of apoptosis markers (cleaved-caspase 3) accompanying RRM1 knockdown. *E*, RRM1 knockdown reduced MIAPaCa-2 cell numbers over 72 h, based upon an MTS assay (Experimental Procedures). *F*, RRM1 knockdown heightened the Gem sensitivity of MIAPaCa-2 cells. The shRNA-transduced cells were treated with a range of Gem concentrations (0–7.5 nM), and cell proliferation was evaluated after 72 h of exposure. *G*,

cells suggest the central role of altered Gem transport and metabolism in establishing GemR. Figure 7 shows an integrated overview of the Gem metabolism pathways overlaid with the fold change in the differentially expressed proteins that were quantified by comparative proteomic analysis of MIA-GR8 and parental MIAPaCa-2 cells. Increased expression of Gem metabolism proteins (RRM1, RRM2, CDA, DCK, DCTD, NT5C, and CMPK1) was observed in MIA-GR8 cells, and clinically, their increased expression correlates significantly with PDAC patient survival (supplemental Fig. S4, supplemental Tables S2 and S3).

Alterations in Gem transport and metabolism pathway enzymes also appear to contribute to establishing the phenotype of GemR cells. ENT1, the primary Gem transporter, was reduced in MIA-GR8 cells (Fig. 7*B*), which would decrease Gem uptake, consistent with previous reports that identified a key role of ENT1 expression levels in determining Gem sensitivity (10). Gem-mediated alterations in the activity of multiple Gem metabolism pathways also cooperate in establishing GemR and can be self-potentiating. The lower expression of DCK and higher expression of NT5C observed in MIA-GR8 cells (Fig. 7*B*) would limit the formation of active Gem gemcitabine monophosphate (dFdCMP+dFdCDP+dFdCTP). DCTD, which deaminates dFdCMP to dFdUMP, was also upregulated. The resulting dFdUMP could be converted into dFdU and exported rapidly from cells by CNT (52, 53), reducing the pool of intracellular dFdU that can be metabolized to dFdUDP and dFdUTP, both of which can mediate cytotoxicity *via* incorporation into DNA and effects on dNTP pools (54, 55). The overall pattern of differential protein expression in MIA-GR8 cells suggest that multiple mechanisms operant in MIA-GR8 cells diminish dFdCMP, which would deplete the active Gem precursor pool. dFdCDP, which is produced from dFdCMP by CMPK1, is a potent suppressor of RNR complex activity and would thereby diminish the cellular dNTP pool produced *via* the nucleoside salvage pathway (16) that competes with Gem incorporation into DNA. CMPK1 was upregulated slightly in MIA-GR8 cells (Fig. 7*B*), possibly because of cellular compensatory signaling that would counter the significant upregulation of the RNR complex observed, which replenishes the competing dNTP pool. Overall, the observed Gem-mediated effects on the activity of Gem-deactivating enzymes and on those that produce phosphorylated Gem species that would compete with dNTP pools could interfere with processes that together can contribute to producing more than 85% of the intracellular Gem undergoing activation by phosphorylation (56).

Proteomic Analysis of Gem Metabolism Pathway Responses to Gem Exposure

The differential expression of proteins associated with Gem transport and metabolism observed in MIA-GR8 *versus* parental MIAPaCa-2 cells motivated an investigation of the relationship between the Gem sensitivity of several PDAC cell lines and their protein-level responses to Gem exposure. The rank-order Gem sensitivity of these cell lines is MIAPaCa-2 > PANC-1 >> MIA-GR8 cells ((57, 58); this study).

In all three cell lines, expression of ENT1, the major Gem uptake transporter (59), increased over the first 48 h of Gem exposure and then declined (Fig. 8*A*), suggesting an initial increase in Gem uptake capacity. Although the initial ENT1 induction was greatest in PANC-1, it declined more rapidly than in MIAPaCa-2, suggesting a more rapid adaptation of the more GemR PANC-1 to reduce Gem uptake. ENT1 induction in MIA-GR8 was minimal and significantly lower than in other cell lines at 48 h of exposure, suggesting that MIA-GR8 had the lowest Gem uptake capacity.

Once cells take up Gem, its activation and conversion to DFdCMP are modulated by DCK, NT5C, and DCTD. DCK was quantifiable in only PANC-1 and MIA-GR8 cells. Whereas PANC-1 upregulated DCK in response to Gem treatment, it did not change in MIA-GR8 (Fig. 8*B*), suggesting its lower capacity for production of dFdCMP. NT5C and DCTD inactivate dFdCMP, producing parental Gem and dFdUMP. MIAPaCa-2 cells downregulated NT5C after 24 to 72 h of Gem exposure, which would preserve dFdCMP and promote increased dFdCDP and dFdUMP, both of which are cytotoxic (Fig. 8*C*). NT5C expression initially increased in PANC-1 cells, which would reduce dFdCMP, but then declined over the following 48 h. NT5C was slightly upregulated after 24 h in MIA-GR8 cells and remained at a higher level than in PANC-1 and MIAPaCa-2, suggesting a more sustained capacity for decreasing dFdCMP. DCTD was relatively unchanged in MIAPaCa-2 cells but was strongly induced in PANC-1 cells after a delay of 24 h (Fig. 8*D*), suggesting increased metabolic inactivation of dFdCMP to dFdUMP as a dynamic response to

representative bright-field images of migrating MIAPaCa-2 cells transduced with scrambled- or RRM1-specific shRNAs; *H*, quantification of cells migrating in a Transwell assay shows that RRM1 knockdown reduces MIAPaCa-2 cell migration. *I*, comparison of RRM1 mRNA expression in normal pancreas *versus PDAC* tumors. Transcriptomics data for 176 PDAC patient tumors were obtained from The Cancer Genome Atlas (TCGA) database (https://portal.gdc.cancer.gov/) and data for 247 normal pancreata were obtained from the Genotype-Tissue Expression (GTEx) database (https://www.gtexportal.org/). The extracted values were normalized to TPM (Transcripts Per Million) for comparison; normal pancreas tissues had significantly higher RRM1 expression than PDAC tumors ($p = 0.002$) at the transcriptional level. *J*, Kaplan–Meier plots of PDAC patient survival stratified by high (*red*, upper 30%) *versus* low (*green*, lower 30%) expression of RRM1. The plots were created using LOGpc (http://bioinfo.henu.edu.cn/DatabaseList.jsp) using clinical RNA-seq data from TCGA database (https://www.cancer.gov/tcga). Data shown are mean ± SD. $^{*}p < 0.05$, $^{**}p < 0.01$, $^{***}p < 0.001$. ns, not significant. Gem, gemcitabine; GemR, gemcitabine resistance; PDAC, pancreatic adenocarcinoma; RRM1: ribonucleoside-diphosphate reductase large subunit, RRM2: ribonucleoside-diphosphate reductase subunit M2.

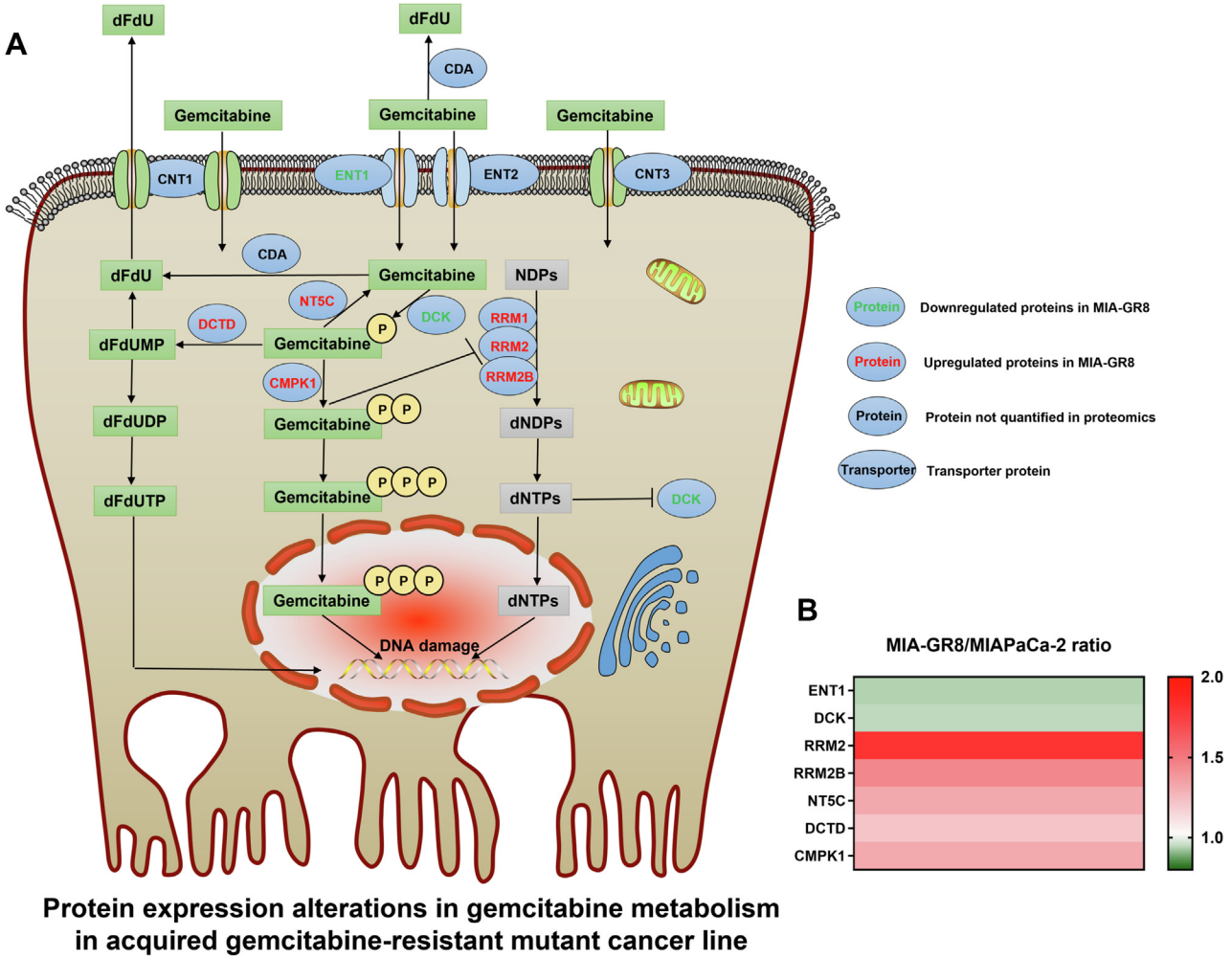

FIG. 7. **Protein expression changes in Gem metabolism pathways in MIA-GR8 cells.** *A*, Gem metabolism network in PDAC cells. Quantified proteins that were downregulated in MIA-GR8 relative to parental MIAPaCa-2 cells are indicated in *green font*, and *red font* represents quantified proteins that were upregulated. Gem is taken up by transporters (ENT1, ENT2, CNT1, CNT3) and metabolized by several key enzymes, including CDA, DCTD, NT5C, DCK, RRM1, RRM2, RRM2B, and CMPK1. Deamination of extracellular Gem by CDA transforms Gem into inactive dFdU. Conversion of the Gem prodrug to active Gem triphosphate requires sequential phosphorylation by multiple enzymes, including DCK, NT5C, and CMPK1. DCK mediates the conversion of parental Gem to dFdCMP, which is a rate-limiting catalyzation step, and NT5C reverses this step by dephosphorylating dFdCMP. DCTD, which deaminates dFdCMP to dFdUMP, was converted into dFdU and exported rapidly from cells by CNT1. Intracellular dFdU can be metabolized to dFdUDP and dFdUTP, both of which can mediate cytotoxicity *via* incorporation into DNA and effects on dNTP pools. The RNR complex consists of RRM1, RRM2, and RRM2B and catalyzes the sequential conversion of NDPs into dNTPs. Gem metabolite dFdCTP competes with NTPs for DNA incorporation. CDA, ENT2, CNT1, and CNT3 were not quantified in the proteomic analysis. *B*, heat-map of protein expression changes associated with Gem metabolism and their magnitude in GemR MIA-GR8 cells. The average expression profiles of Gem transporters and metabolizing enzymes in nearly confluent MIA-GR8 GemR cells at two time points (day 0 prior to plating and day 4 after plating) were normalized by the average expression of the same proteins in MIAPaCa-2 parental cells. CDA, cytidine deaminase; CMPK1, cytidine monophosphate kinase 1; CNT1, solute carrier family 28 member 1; CNT3, solute carrier family 28 member 3; DCK: deoxycytidine kinase; DCTD, deoxycytidylate deaminase; dFdCDP, gemcitabine diphosphate; dFdCMP, gemcitabine monophosphate; dFdCTP, gemcitabine triphosphate; dFdU, difluorodeoxyuridine; ENT1: human equilibrative transporter 1; ENT2, solute carrier family 29 member 2; FdUMP, deoxyfluorouridine monophosphate; Gem, gemcitabine; NT5C, 5′-nucleotidase; PDAC, pancreatic adenocarcinoma; RRM1: ribonucleoside-diphosphate reductase large subunit, RRM2: ribonucleoside-diphosphate reductase subunit M2, RRM2B: ribonucleotide-diphosphate reductase subunit M2 B.

drug exposure. In contrast, DCTD in MIA-GR8 declined over 24 to 72 h and was significantly lower than in MIAPaCa-2 and PANC-1, possibly because of a reduction in dFdCMP; by 96 h, it returned to baseline. The baseline abundance of CMPK1, which phosphorylates dFdCMP, was approxmately 1.2-fold higher in MIA-GR8 than in MIAPaCa-2 (Fig. 7*B*), but MIA-GR8 downregulated CMPK1 by approxmately 30% in the first 24 h of exposure to levels significantly below those of the

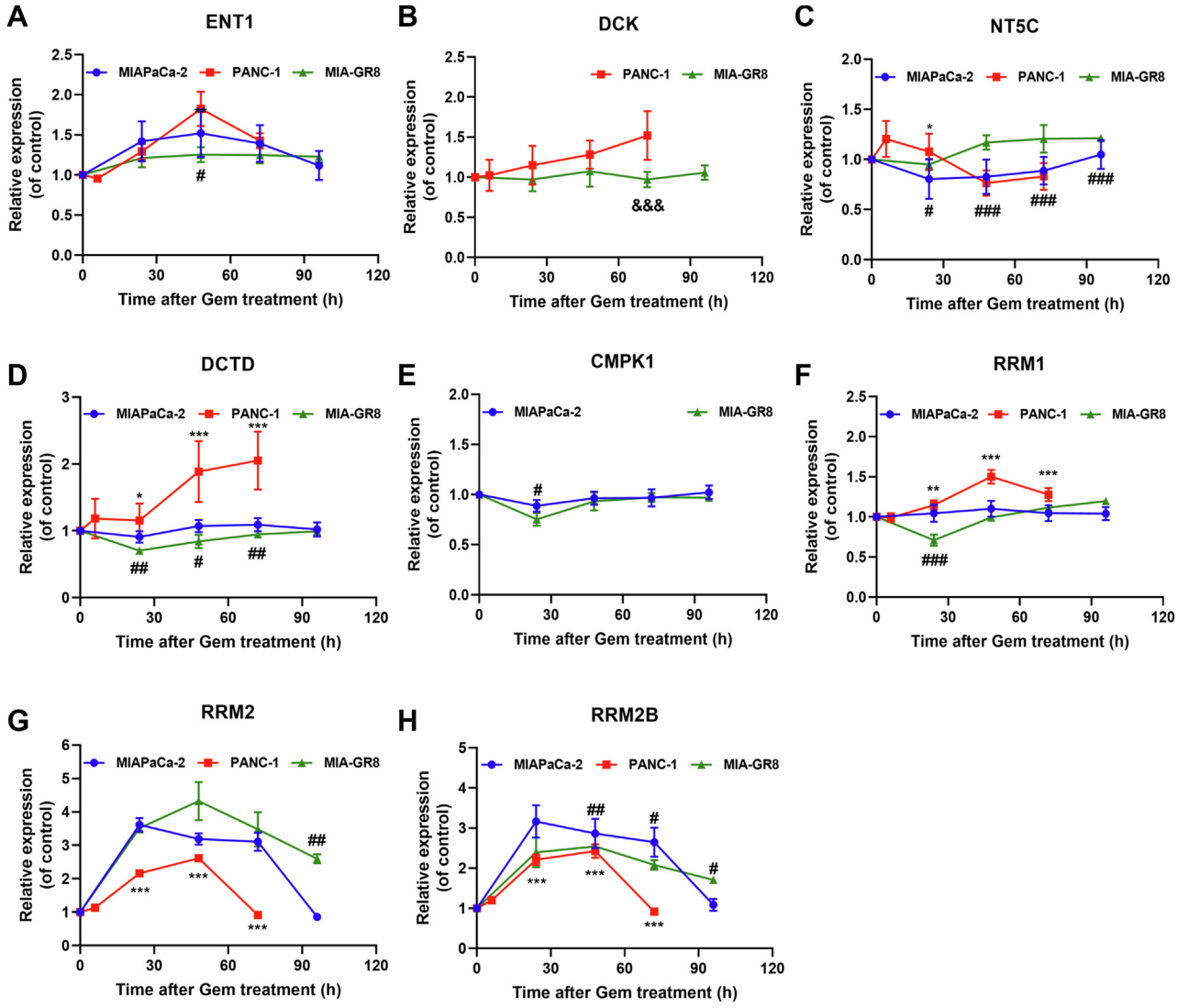

FIG. 8. **Temporal expression changes of proteins associated with Gem metabolism during Gem exposure of PDAC cell lines.** Meta-analysis of data from multiple global proteomic analyses enabled comparison of temporal responses of PDAC cell lines to Gem exposure. In (31) PANC-1 cells were exposed in triplicate to 20 nM Gem over 0 to 72 h. In the experiments performed here, triplicate MIAPaCa-2 cell samples were exposed to 7.5 nM Gem over 0 to 96 h, and MIA-GR8 cells were exposed to 1 μM Gem. At the indicated time points, cells were harvested and subjected to quantitative proteomic analysis. Data are normalized to drug-free controls at time 0. The proteins associated with Gem metabolism that were quantified in these 3 cell lines included (*A*) ENT1, (*B*) DCK, (*C*) NT5C, (*D*) DCTD, (*E*), CMPK1, (*F*) RRM1, (*G*) RRM2, and (*H*) RRM2B. *B*, DCK was not quantified in MIAPaCa-2 cells, and (*E*) CMPK1 was not quantified in PANC-1 cells. Data shown are mean ± SD. Symbols: comparison between MIAPaCa-2 and PANC-1 cells: $^{*}p < 0.05$, $^{**}p < 0.01$, $^{***}p < 0.001$; comparison between MIAPaCa-2 and MIA-GR8 cells: #$p < 0.05$, ##$p < 0.01$, ###$p < 0.001$; comparison between PANC-1 and MIA-GR8 cells: &$p < 0.05$, &&$p < 0.01$, &&&$p < 0.001$. DCK: deoxycytidine kinase; DCTD, deoxycytidylate deaminase; ENT1: human equilibrative transporter 1; Gem, gemcitabine; GemR, gemcitabine resistance; NT5C, 5′-nucleotidase; PDAC, pancreatic adenocarcinoma; RRM1, ribonucleoside-diphosphate reductase large subunit; RRM2, ribonucleoside-diphosphate reductase subunit M2; RRM2B, ribonucleotide-diphosphate reductase subunit M2 B.

more Gem-sensitive MIAPaCa-2 (Fig. 8*E*). This response would have the effect of reducing the phosphorylation necessary to activate Gem.

RRM1 expression did not change appreciably in MIAPaCa-2 cells over 96 h of Gem exposure but did increase rapidly over 48 h in PANC-1 cells (Fig. 8*F*), consistent with its greater GemR. In MIA-GR8 cells, 24 h of Gem exposure at a relatively high concentration transiently downregulated RRM1 (Fig. 8*F*). Despite this 25 to 30% decrease in RRM1 expression, its abundance in MIA-GR8 cells remained 15-fold higher than in MIAPaCa-2 cells, which would maintain MIA-GR8 cell proliferation and survival. RRM1 expression in MIA-GR8 cells then returned to baseline by 48 h, suggesting that the cells possess a rapid, adaptative response mechanism to counteract

suppression of RRM1 by high Gem exposure. Thus the observed magnitude of downregulation of RRM1 may not impact the overall GemR phenotype of MIA-GR8. In all PDAC cell lines, the expression of RRM2 and RRM2B exhibited bell-shape patterns in response to Gem exposure (Fig. 8, *G* and *H*), implicating an early DNA repair response to reverse Gem-mediated DNA damage (60, 61). Among the three cell lines, RRM2 induction was greatest in MIA-GR8 cells, suggesting it possessed the highest capacity for DNA repair (Fig. 8*G*).

DISCUSSION

Gem is the mainstay of a prevalent, standard-of-care chemotherapy regimen for PDAC, one of the most lethal cancers (62). Tumors that are initially sensitive to Gem-based therapies become drug-resistant, resulting in only a modest survival improvement. Therefore, developing a more complete understanding of GemR and establishing a rational basis for the design of effective approaches to overcome GemR, remain a major clinical challenge (63). Multiple GemR mechanisms have been documented at molecular, enzymatic, cellular, and physiological levels (5–7, 11, 14–16, 18, 42, 63–72), and numerous prognostic markers have been proposed to predict the emergence of GemR and patient Gem response (13, 18, 19). Here, we investigated the molecular mechanisms underlying acquired GemR using a global differential proteomic analysis approach for hypothesis generation and testing. The *IonStar* proteomic analysis workflow enabled quantification of a much larger number of differentially expressed proteins in GemR cells, at a high level of stringency, than achieved in previous studies in the field (21, 24–26).

In order to evaluate GemR against a consistent genetic background, we derived a family of GemR clones from the Gem-sensitive MIAPaCa-2 PDAC cell line. Clone #8 (MIA-GR8) was one of several highly resistant clones derived. Our rationale in selecting this clone for detailed phenotypic and proteomic analysis was based upon the hypothesis that the sheer-magnitude change in Gem sensitivity in the clonal lines obtained would involve the emergence of multiple cooperating GemR mechanisms. MIA-GR8 exhibited the greatest degree of GemR among these lines and retained its tumorigenic- and Gem-resistant properties *in vivo*. Phenotypically, MIA-GR8 cells exhibited a mesenchymal appearance, with enhanced expression of mesenchymal markers compared to parental cells, which was consistent with their increased *in vitro* invasiveness and drug resistance. MIA-GR8 cells also grew more slowly than parental cells, and a significant fraction of cells accumulated in G_0/G_1. Together, these characteristics would reduce S phase incorporation of Gem into DNA. MIA-GR8 tumors also grew more slowly *in vivo* than did the parental MIAPaCa-2 tumors. Quantitative differential proteomic analysis showed that multiple biological processes associated with cell proliferation and motility were altered in MIA-GR8 cells. S100A4, a regulator of PDAC cell proliferation, was the most downregulated protein in MIA-GR8 cells, consistent with the reduced proliferation rate observed *in vitro* and *in vivo*, which would represent a protective adaptation to minimize the effects of cytotoxic agents that predominantly target rapid cell growth. However, the role of S100A4 in drug resistance may vary depending on multiple factors. In colon cancer cells, overexpression of S100A4 conferrs resistance to methotrexate (73), but a study of gastric cancer reported that neither overexpression nor knockdown of S100A4 affected cell response to six commonly used cytotoxic agents (74). In PDAC, downregulation of S100A4 was observed to slow cell proliferation (75), and overexpression of S100A4 increased invasiveness (76). Downregulation of S100A4 in MIA-GR8 cells suggests that its contribution to GemR may be *via* reduction of cell proliferation.

The slower proliferation rate of MIA-GR8 cells was also consistent with the observed reduction in energy generation from glycolysis and mitochondrial respiration. Differential analysis showed that proteins related to cellular metabolism represented the predominant functionally annotated biological process group altered in MIA-GR8 cells compared to parental MIAPaCa-2 cells. Notably, RRM1, which plays a major role as a determinant of Gem sensitivity (18, 19, 77, 78), was the most upregulated protein in the group. Increased RRM1 expression was observed in all nine GemR clones isolated, suggesting a key role of altered Gem metabolism in GemR. The functional role of RRM1 in GemR was validated and extended experimentally with the observation that a reduction in RRM1 abundance enhanced PDAC cell sensitivity to Gem and decreased cell proliferation and migration. The clinical implications of these findings were investigated, and TCGA database analysis showed that higher RRM1 expression is related to poorer survival of PDAC patients. Considering the elevated expression of RRM1 in PDAC tumors compared to the normal pancreas, RRM1 would appear to be a promising target for drug combinations to overcome GemR.

Differential proteomic analysis identified additional metabolic alterations in MIA-GR8 cells that would impact drug metabolism. Key enzymes relating to altered Gem metabolism pathways included the ENT/CNT transporter family, as well as DCK, NT5C, DTCD, CMPK1, and other RNR complex proteins. Downregulation of ENT1 in MIA-GR8 cells would decrease Gem uptake (79–81), and downregulation of DCK, in parallel with upregulation of NT5C and DCTD, would decrease the intracellular abundance of dFdCMP, a key precursor of the triphosphorylated species that undergo DNA incorporation (16, 63). The RNR complex was also upregulated in MIA-GR8 cells, suggesting enhanced DNA repair mechanisms (60) and a weaker capacity for Gem incorporation into DNA (18, 19, 78). Thus, the overall pattern of protein-level responses of the MIA-GR8 cell line suggested that sustained Gem exposure selected for adaptations in protein expression that would reduce the intracellular concentrations of active Gem metabolites and elevate baseline expression of proteins in Gem

metabolism pathways that would contribute to the GemR phenotype.

Proteins comprising 'drug-response mechanisms' were altered significantly in MIA-GR8 cells. Therefore, we tested the hypothesis that additional GemR cell lines may possess or develop similar adaptations to reduce Gem-induced stress, such as modulation of proteins in Gem transport and metabolism pathways that could decrease active Gem metabolites. Multiple PDAC cell lines, showing a range of intrinsic GemR, were analyzed. These included parental MIAPaCa-2, PANC-1, and MIA-GR8 cells. Protein expression patterns suggested that PANC-1 and MIA-GR8 cells would have decreased capacity for Gem accumulation compared to MIAPaCa-2 cells. However, the molecular mechanisms of adaption to Gem may differ; in the intrinsically GemR PANC-1 cell line (57, 58), the predominating proteome-level changes tended toward those that would decrease cellular accumulation of Gem, based upon a sharper but delayed upregulation of DCTD, as well as greater upregulation of RRM1. Both responses are consistent with a relatively GemR phenotype. The highly GemR MIA-GR8 cell line also showed proteomic changes that would confer a decreased capacity to accumulate Gem, based upon attenuated induction of ENT1, unchanged DCK, a delayed but greatly increased NT5C, which would counter RRM1 suppression by Gem, and a robust increase in RRM2. Thus, global proteomic analysis provided considerable comparative insights into GemR mechanisms of PDAC cells and generated additional testable hypotheses relating to the contribution of specific protein-level responses to overall Gem sensitivity.

Our approach was to generate a series of GemR cell lines from the relatively Gem-sensitive MIAPaCa-2 cell line, which would be analogous to the clinical situation in which treatment-naïve patients who initially have moderately Gem-responsive tumors become resistant as a consequence of therapeutic Gem exposure. Previous comparative proteomic analyses have investigated GemR in various cancer models. They differ in study objectives and experimental design, employ different parental cell lines and patterns of drug exposure, and utilize different analytical approaches and data interpretation. Despite these differences in focus and methodology, some commonalities have emerged from the study of GemR PDAC cell lines. A previous work (82) generated GemR cells from the intrinsically GemR cell line PANC-1 and reported a number of observations similar to those presented here. Although the magnitude of change in IC_{50} reported previously was 6-fold, compared to the approximately 100-fold reduction in Gem sensitivity reported here, that prior work (82) did report alterations in acquired-GemR lines in the expression of proteins associated with cell division, proliferation, and migration, particularly in the microtubule-associated proteins that were a focus of that study. However, the reported fold changes in expression of proteins quantified differ in magnitude from this study and in some cases, in the direction of change. This may reflect the use of intrinsically drug-resistant parental cell lines *versus* more drug-sensitive parental cell lines, as employed here, for the generation of GemR mutants. The work presented here also provided a number of functional experimental confirmations and validated the role of Gem metabolic effectors such as RRM1 in the GemR cells. Where concordance exists in the two studies, it raises confidence in the capability of quantitative protein-level expression analysis to provide valuable insights into drug resistance mechanisms. Where they differ, there is an opportunity to broaden our understanding of the diversity and interplay of pharmacological response systems in PDAC.

A limitation of the present study is that the depth of ancillary experimental validation and informatic investigation of hypotheses necessary to present an integrated picture from the diverse and interacting mechanisms of GemR observed precludes a similarly detailed investigation of all of the acquired-GemR clones we developed. Some data show the additional clones share characteristics of the MIA-GR8 clone, and the comparative investigation of the intrinsically GemR PANC-1 *versus* the relatively Gem-sensitive MIAPaCa-2 provides additional evidence that GemR mechanisms involving metabolic alterations are shared across other PDAC lines. However, with the data obtained and hypotheses generated, ongoing and future work should transition to evaluating the clinical diversity of PDAC resistance mechanisms, which are captured in libraries of patient-derived xenograft (PDX) models developed by numerous groups, in which PDAC tumor fragments have been implanted directly into immunodeficient mice and have never been selected for growth *in vitro*. Each PDAC PDX isolate recapitulates the full complexity of the clinical disease and applying this comprehensive differential proteomic analysis approach to multiple PDAC PDX models, for which clinical outcomes are known, will provide the opportunity to extend our understanding of drug resistance mechanisms as they exist or develop clinically. Such work is guided by the hypotheses and findings of the present work with the MIA-GR8 cell line, which has enabled us to explore in considerable degree the complexity and parallel development of multiple, interrelated GemR mechanisms.

A notable caveat to the interpretation of quantitative proteomic analysis results is that the correlation between statistically significant fold changes in protein abundance and biologically significant effects on function are typically unknown, necessitating functional validations. By their nature, very large datasets themselves present challenges. Numerous other biological processes showed proteome-level changes as a result of Gem exposure, including vesicular transport, lysosomal activity, and synthesis of biomass. Although the focused investigation presented here provides experimental validation and extension of numerous findings, we could not pursue all leads provided by the data. Nonetheless, global

differential proteomic analysis was successful in hypothesis generation and testing key hypotheses. In future studies, our depth of understanding of cellular drug response networks could be improved by the integration of large-scale, comprehensive analysis of posttranslational modifications, given reports that changes in phosphorylation and acetylation can impact phenotypic aspects of GemR *via* changes in signal transduction activity (69, 70, 82–85).

In conclusion, quantitative global proteomic analysis identified a wide range of GemR mechanisms within the large number of differentially expressed proteins quantified in mutant, highly GemR cell lines derived from a drug-sensitive parental PDAC cell line and in PDAC cell lines that vary in their intrinsic sensitivity to Gem exposure. The findings show that GemR cells modulate multiple pathways to adapt to Gem-induced stress. Responses in Gem metabolism pathways were identified as a major contributor to GemR and changes in the expression of key proteins both influence Gem responsiveness and suggest that targeting Gem metabolism pathways with novel therapeutic combinations may improve Gem efficacy.

DATA AVAILABILITY

Two mass spectrometry proteomics datasets are deposited at to the ProteomeXchange Consortium *via* the PRIDE partner repository with the dataset identifiers PXD030861 (dataset of MIAPaCa-2 cell responses to Gem) and PXD030859 (dataset of MIA-GR8 cell responses to Gem, with a comparative proteomic analysis of MIA-GR8 and MIAPaCa-2). Detailed information on protein identification (accession # in the Human Uniprot database, # of distinct peptides, and % coverage of each protein), quantification, and peptide information is available in supplemental Tables S4–S12. These materials are available online:

MIAPaCa-2 Data

Submission details:

Project Name: MIA PaCa-2 cells treated with Gemcitabine Project accession: PXD030861 Project DOI: 10.6019/PXD030861

MIA-GR8 Data

Submission details:

Project Name: R8 (Gem resistant cell line) treated with Gem Project accession: PXD030859 Project DOI: 10.6019/PXD030859

Supplemental data—This article contains supplemental data (28, 29, 33, 35, 37, 86).

Acknowledgments—We thank Drs X. Zhu and X. Miao for generating the proteomics datasets.

Funding and additional information—This work was supported by the US National Institutes of Health (NIH)/National Cancer Institute (NCI) grants R01CA198096 to R.M.S., R21CA168454 to R.M.S. and J.Q., NIH grant GM131800 to W.J.J., Roswell Park Alliance Foundation and NIH grants RO3 CA205178 to E.K., utilized shared resources supported by Comprehensive Cancer Center Support Grant NIH/NCI P30CA016056 to Roswell Park Comprehensive Cancer Center, and received seed support from NIH/NCATS (National Center for Advancing Translational Sciences) award UL1TR001412 to the University at Buffalo, State University of New York. The content is solely the responsibility of the authors and does not necessarily represent the official views of the National Institutes of Health.

Author contributions—Q. L., J. Q., and R. M. S. conceptualization; Q. L. data curation; Q. L. formal analysis; Q. L., S. S., Z. Q., S. S. R., A. S., E. S. K., and R. M. S. investigation; Q. L. and S. S. methodology; Q. L. and R. M. S. project administration; Q. L., Z. Q., S. S. R., A. S. validation; Q. L. visualization; Q. L. and R. M. S. writing-original draft; Q. L., S. S., S. S. R., W. J. J., E. S. K., J. Q., and R. M. S. writing-review & editing; W. J. J., E. S. K., and J. Q. resources; W. J. J. software; W. J. J., E. S. K., J. Q., and R. M. S. funding acquisition; E. S. K., J. Q., and R. M. S. supervision.

Conflict of interest—The authors declare no competing interests.

Abbreviations—The abbreviations used are: AACT (SERPINA3), serpin family A member 3; ADLH2, aldehyde dehydrogenase 2 family member; ATP7B, ATPase copper transporting beta; CALB, calbindin 2; CATD (CTSD), cathepsin D; CDA, cytidine deaminase; CMPK1, cytidine monophosphate kinase 1; CNT1, solute carrier family 28 member 1; CNT3, solute carrier family 28 member 3; CV, coefficient of variation; dFdCDP, gemcitabine diphosphate; dFdCMP, gemcitabine monophosphate; dFdCTP, gemcitabine triphosphate; dFdU, difluorodeoxyuridine; FdUMP, deoxyfluorouridine monophosphate; DCK, deoxycytidine kinase; DCTD, deoxycytidylate deaminase; dNTP, deoxyribonucleotide triphosphate; ECAR, extracellular acidification rate; ENT1, human equilibrative transporter 1; ENT2, solute carrier family 29 member 2; EMT, epithelial–mesenchymal transition; FDR, false discovery rate; FETUA(AHSG), alpha 2-HS glycoprotein; Gem, gemcitabine; GemR, gemcitabine resistance; GEL2 (GSN), gelsolin; KCRB (CKB), creatine kinase B; NT5C, 5′-nucleotidase; NDK1, nucleoside diphosphate kinase 1; OCR, oxygen consumption rate; PDAC, pancreatic adenocarcinoma; RO52 (TRIM21), tripartite motif containing 21; RNR, ribonucleotide reductase; RRM1, ribonucleoside-diphosphate reductase large subunit; RRM2, ribonucleoside-diphosphate reductase subunit M2; RRM2B, ribonucleotide-diphosphate reductase subunit M2 B; S100A4, S100 calcium binding protein A4; STIM1, stromal interaction molecule 1; TYMS, thymidylate synthetase.

Received November 2, 2021, and in revised form, August 21, 2022
Published, MCPRO Papers in Press, September 7, 2022, https://doi.org/10.1016/j.mcpro.2022.100409

REFERENCES

1. Siegel, R. L., Miller, K. D., Fuchs, H. E., and Jemal, A. (2021) Cancer statistics, 2021. *CA Cancer J Clin* **71**, 7–33
2. Rahib, L., Wehner, M. R., Matrisian, L. M., and Nead, K. T. (2021) Estimated projection of US cancer incidence and death to 2040. *JAMA Netw. Open* **4**, e214708
3. Vaccaro, V., Sperduti, I., and Milella, M. (2011) FOLFIRINOX versus gemcitabine for metastatic pancreatic cancer. *N. Engl. J. Med.* **365**, 768–769
4. Von Hoff, D. D., Ervin, T., Arena, F. P., Chiorean, E. G., Infante, J., Moore, M., *et al*. (2013) Increased survival in pancreatic cancer with nab-paclitaxel plus gemcitabine. *N. Engl. J. Med.* **369**, 1691–1703
5. Hessmann, E., Patzak, M. S., Klein, L., Chen, N., Kari, V., Ramu, I., *et al*. (2018) Fibroblast drug scavenging increases intratumoural gemcitabine accumulation in murine pancreas cancer. *Gut* **67**, 497–507
6. Olive, K. P., Jacobetz, M. A., Davidson, C. J., Gopinathan, A., McIntyre, D., Honess, D., *et al*. (2009) Inhibition of Hedgehog signaling enhances delivery of chemotherapy in a mouse model of pancreatic cancer. *Science* **324**, 1457–1461
7. Neesse, A., Michl, P., Frese, K. K., Feig, C., Cook, N., Jacobetz, M. A., *et al*. (2011) Stromal biology and therapy in pancreatic cancer. *Gut* **60**, 861–868
8. Binenbaum, Y., Na'ara, S., and Gil, Z. (2015) Gemcitabine resistance in pancreatic ductal adenocarcinoma. *Drug Resist. Updat.* **23**, 55–68
9. Shibue, T., and Weinberg, R. A. (2017) EMT, CSCs, and drug resistance: the mechanistic link and clinical implications. *Nat. Rev. Clin. Oncol.* **14**, 611–629
10. Namba, T., Kodama, R., Moritomo, S., Hoshino, T., and Mizushima, T. (2015) Zidovudine, an anti-viral drug, resensitizes gemcitabine-resistant pancreatic cancer cells to gemcitabine by inhibition of the Akt-GSK3beta-Snail pathway. *Cell Death Dis.* **6**, e1795
11. Wang, Z., Li, Y., Kong, D., Banerjee, S., Ahmad, A., Azmi, A. S., *et al*. (2009) Acquisition of epithelial-mesenchymal transition phenotype of gemcitabine-resistant pancreatic cancer cells is linked with activation of the notch signaling pathway. *Cancer Res.* **69**, 2400–2407
12. Porter, R. L., Magnus, N. K. C., Thapar, V., Morris, R., Szabolcs, A., Neyaz, A., *et al*. (2019) Epithelial to mesenchymal plasticity and differential response to therapies in pancreatic ductal adenocarcinoma. *Proc. Natl. Acad. Sci. U. S. A.* **116**, 26835–26845
13. Rauchwerger, D. R., Firby, P. S., Hedley, D. W., and Moore, M. J. (2000) Equilibrative-sensitive nucleoside transporter and its role in gemcitabine sensitivity. *Cancer Res.* **60**, 6075–6079
14. Farrell, J. J., Elsaleh, H., Garcia, M., Lai, R., Ammar, A., Regine, W. F., *et al*. (2009) Human equilibrative nucleoside transporter 1 levels predict response to gemcitabine in patients with pancreatic cancer. *Gastroenterology* **136**, 187–195
15. Weizman, N., Krelin, Y., Shabtay-Orbach, A., Amit, M., Binenbaum, Y., Wong, R. J., *et al*. (2014) Macrophages mediate gemcitabine resistance of pancreatic adenocarcinoma by upregulating cytidine deaminase. *Oncogene* **33**, 3812–3819
16. Alvarellos, M. L., Lamba, J., Sangkuhl, K., Thorn, C. F., Wang, L., Klein, D. J., *et al*. (2014) PharmGKB summary: gemcitabine pathway. *Pharmacogenet. Genomics* **24**, 564–574
17. Lin, Q., Qian, Z., Jusko, W. J., Mager, D. E., Ma, W. W., and Straubinger, R. M. (2021) Synergistic pharmacodynamic effects of gemcitabine and fibroblast growth factor receptor inhibitors on pancreatic cancer cell cycle kinetics and proliferation. *J. Pharmacol. Exp. Ther.* **377**, 370–384
18. Akita, H., Zheng, Z., Takeda, Y., Kim, C., Kittaka, N., Kobayashi, S., *et al*. (2009) Significance of RRM1 and ERCC1 expression in resectable pancreatic adenocarcinoma. *Oncogene* **28**, 2903–2909
19. Jordheim, L. P., Seve, P., Tredan, O., and Dumontet, C. (2011) The ribonucleotide reductase large subunit (RRM1) as a predictive factor in patients with cancer. *Lancet Oncol.* **12**, 693–702
20. Moore, M. J., Goldstein, D., Hamm, J., Figer, A., Hecht, J. R., Gallinger, S., *et al*. (2007) Erlotinib plus gemcitabine compared with gemcitabine alone in patients with advanced pancreatic cancer: a phase III trial of the National Cancer Institute of Canada Clinical Trials Group. *J. Clin. Oncol.* **25**, 1960–1966
21. Mori-Iwamoto, S., Kuramitsu, Y., Ryozawa, S., Taba, K., Fujimoto, M., Okita, K., *et al*. (2008) A proteomic profiling of gemcitabine resistance in pancreatic cancer cell lines. *Mol. Med. Rep.* **1**, 429–434
22. Kuramitsu, Y., Wang, Y., Taba, K., Suenaga, S., Ryozawa, S., Kaino, S., *et al*. (2012) Heat-shock protein 27 plays the key role in gemcitabine-resistance of pancreatic cancer cells. *Anticancer Res.* **32**, 2295–2299
23. Chen, R., Lai, L. A., Sullivan, Y., Wong, M., Wang, L., Riddell, J., *et al*. (2017) Disrupting glutamine metabolic pathways to sensitize gemcitabine-resistant pancreatic cancer. *Sci. Rep.* **7**, 7950
24. Fujimura, Y., Ikenaga, N., Ohuchida, K., Setoyama, D., Irie, M., Miura, D., *et al*. (2014) Mass spectrometry-based metabolic profiling of gemcitabine-sensitive and gemcitabine-resistant pancreatic cancer cells. *Pancreas* **43**, 311–318
25. Kim, Y., Han, D., Min, H., Jin, J., Yi, E. C., and Kim, Y. (2014) Comparative proteomic profiling of pancreatic ductal adenocarcinoma cell lines. *Mol. Cells* **37**, 888–898
26. Chen, Y. W., Liu, J. Y., Lin, S. T., Li, J. M., Huang, S. H., Chen, J. Y., *et al*. (2011) Proteomic analysis of gemcitabine-induced drug resistance in pancreatic cancer cells. *Mol. Biosyst.* **7**, 3065–3074
27. Wang, X., Niu, J., Li, J., Shen, X., Shen, S., Straubinger, R. M., *et al*. (2018) Temporal effects of combined birinapant and paclitaxel on pancreatic cancer cells investigated via large-scale, ion-current-based quantitative proteomics (IonStar). *Mol. Cell. Proteomics* **17**, 655–671
28. Shen, X., Shen, S., Li, J., Hu, Q., Nie, L., Tu, C., *et al*. (2018) IonStar enables high-precision, low-missing-data proteomics quantification in large biological cohorts. *Proc. Natl. Acad. Sci. U. S. A.* **115**, E4767–E4776
29. Shen, X., Shen, S., Li, J., Hu, Q., Nie, L., Tu, C., *et al*. (2017) An IonStar experimental strategy for MS1 ion current-based quantification using ultrahigh-field orbitrap: reproducible, in-depth, and accurate protein measurement in large cohorts. *J. Proteome Res.* **16**, 2445–2456
30. Lin, Q., He, Y., Wang, X., Zhang, Y., Hu, M., Guo, W., *et al*. (2020) Targeting pyruvate carboxylase by a small molecule suppresses breast cancer progression. *Adv. Sci. (Weinh.)* **7**, 1903483
31. Zhu, X., Shen, X., Qu, J., Straubinger, R. M., and Jusko, W. J. (2018) Proteomic analysis of combined gemcitabine and birinapant in pancreatic cancer cells. *Front Pharmacol.* **9**, 84
32. Shen, S., An, B., Wang, X., Hilchey, S. P., Li, J., Cao, J., *et al*. (2018) Surfactant cocktail-aided extraction/precipitation/on-pellet digestion strategy enables efficient and reproducible sample preparation for large-scale quantitative proteomics. *Anal. Chem.* **90**, 10350–10359
33. Ma, Z. Q., Dasari, S., Chambers, M. C., Litton, M. D., Sobecki, S. M., Zimmerman, L. J., *et al*. (2009) IDPicker 2.0: improved protein assembly with high discrimination peptide identification filtering. *J. Proteome Res.* **8**, 3872–3881
34. Shen, X., Hu, Q., Li, J., Wang, J., and Qu, J. (2015) Experimental null method to guide the development of technical procedures and to control false-positive discovery in quantitative proteomics. *J. Proteome Res.* **14**, 4147–4157
35. Huang, D. W., Sherman, B. T., and Lempicki, R. A. (2009) Systematic and integrative analysis of large gene lists using DAVID bioinformatics resources. *Nat. Protoc.* **4**, 44–57
36. Cancer Genome Atlas Research Network. (2017) Integrated genomic characterization of pancreatic ductal adenocarcinoma. *Cancer Cell* **32**, 185–203.e13
37. Zhang, G., Wang, Q., Yang, M., Yao, X., Qi, X., An, Y., *et al*. (2020) OSpaad: an online tool to perform survival analysis by integrating gene expression profiling and long-term follow-up data of 1319 pancreatic carcinoma patients. *Mol. Carcinog.* **59**, 304–310
38. Liu, J., Lichtenberg, T., Hoadley, K. A., Poisson, L. M., Lazar, A. J., Cherniack, A. D., *et al*. (2018) An integrated TCGA pan-cancer clinical data resource to drive high-quality survival outcome analytics. *Cell* **173**, 400–416.e11
39. Keen, J. C., and Moore, H. M. (2015) The genotype-tissue expression (GTEx) project: linking clinical data with molecular analysis to advance personalized medicine. *J. Pers Med.* **5**, 22–29
40. Lonsdale, J., Thomas, J., Salvatore, M., Phillips, R., Lo, E., Shad, S., *et al*. (2013) The genotype-tissue expression (GTEx) project. *Nat. Genet.* **45**, 580–585

41. Carithers, L. J., and Moore, H. M. (2015) The genotype-tissue expression (GTEx) project. *Biopreserv. Biobank* **13**, 307–308
42. Hong, S. P., Wen, J., Bang, S., Park, S., and Song, S. Y. (2009) CD44-positive cells are responsible for gemcitabine resistance in pancreatic cancer cells. *Int. J. Cancer* **125**, 2323–2331
43. El Amrani, M., Corfiotti, F., Corvaisier, M., Vasseur, R., Fulbert, M., Skrzypczyk, C., *et al*. (2019) Gemcitabine-induced epithelial-mesenchymal transition-like changes sustain chemoresistance of pancreatic cancer cells of mesenchymal-like phenotype. *Mol. Carcinog.* **58**, 1985–1997
44. Che, P., Yang, Y., Han, X., Hu, M., Sellers, J. C., Londono-Joshi, A. I., *et al*. (2015) S100A4 promotes pancreatic cancer progression through a dual signaling pathway mediated by Src and focal adhesion kinase. *Sci. Rep.* **5**, 8453
45. Boye, K., and Maelandsmo, G. M. (2010) S100A4 and metastasis: a small actor playing many roles. *Am. J. Pathol.* **176**, 528–535
46. Fei, F., Qu, J., Zhang, M., Li, Y., and Zhang, S. (2017) S100A4 in cancer progression and metastasis: a systematic review. *Oncotarget* **8**, 73219–73239
47. Gautam, A., Li, Z. R., and Bepler, G. (2003) RRM1-induced metastasis suppression through PTEN-regulated pathways. *Oncogene* **22**, 2135–2142
48. Gautam, A., and Bepler, G. (2006) Suppression of lung tumor formation by the regulatory subunit of ribonucleotide reductase. *Cancer Res.* **66**, 6497–6502
49. Cao, M. Y., Lee, Y., Feng, N. P., Xiong, K., Jin, H., Wang, M., *et al*. (2003) Adenovirus-mediated ribonucleotide reductase R1 gene therapy of human colon adenocarcinoma. *Clin. Cancer Res.* **9**, 4553–4561
50. Xu, X., Page, J. L., Surtees, J. A., Liu, H., Lagedrost, S., Lu, Y., *et al*. (2008) Broad overexpression of ribonucleotide reductase genes in mice specifically induces lung neoplasms. *Cancer Res.* **68**, 2652–2660
51. Nakahira, S., Nakamori, S., Tsujie, M., Takahashi, Y., Okami, J., Yoshioka, S., *et al*. (2007) Involvement of ribonucleotide reductase M1 subunit overexpression in gemcitabine resistance of human pancreatic cancer. *Int. J. Cancer* **120**, 1355–1363
52. Koolen, S. L., Huitema, A. D., Jansen, R. S., van Voorthuizen, T., Beijnen, J. H., Smit, W. M., *et al*. (2009) Pharmacokinetics of gemcitabine and metabolites in a patient with double-sided nephrectomy: a case report and review of the literature. *Oncologist* **14**, 944–948
53. Hodge, L. S., Taub, M. E., and Tracy, T. S. (2011) Effect of its deaminated metabolite, 2',2'-difluorodeoxyuridine, on the transport and toxicity of gemcitabine in HeLa cells. *Biochem. Pharmacol.* **81**, 950–956
54. Derissen, E. J. B., Huitema, A. D. R., Rosing, H., Schellens, J. H. M., and Beijnen, J. H. (2018) Intracellular pharmacokinetics of gemcitabine, its deaminated metabolite 2',2'-difluorodeoxyuridine and their nucleotides. *Br. J. Clin. Pharmacol.* **84**, 1279–1289
55. Mini, E., Nobili, S., Caciagli, B., Landini, I., and Mazzei, T. (2006) Cellular pharmacology of gemcitabine. *Ann. Oncol.* **17 Suppl 5**, V7–V12
56. Heinemann, V., Xu, Y. Z., Chubb, S., Sen, A., Hertel, L. W., Grindey, G. B., *et al*. (1992) Cellular elimination of 2',2'-difluorodeoxycytidine 5'-triphosphate: a mechanism of self-potentiation. *Cancer Res.* **52**, 533–539
57. Huai, Y., Zhang, Y., Xiong, X., Das, S., Bhattacharya, R., and Mukherjee, P. (2019) Gold nanoparticles sensitize pancreatic cancer cells to gemcitabine. *Cell Stress* **3**, 267–279
58. Cao, L. P., Song, J. L., Yi, X. P., and Li, Y. X. (2013) Double inhibition of NF-kappaB and XIAP via RNAi enhances the sensitivity of pancreatic cancer cells to gemcitabine. *Oncol. Rep.* **29**, 1659–1665
59. Vincenzi, B., Stacchiotti, S., Collini, P., Pantano, F., Rabitti, C., Perrone, G., *et al*. (2017) Human equilibrative nucleoside transporter 1 gene expression is associated with gemcitabine efficacy in advanced leiomyosarcoma and angiosarcoma. *Br. J. Cancer* **117**, 340–346
60. Kuo, M. L., Sy, A. J., Xue, L., Chi, M., Lee, M. T., Yen, T., *et al*. (2012) RRM2B suppresses activation of the oxidative stress pathway and is up-regulated by p53 during senescence. *Sci. Rep.* **2**, 822
61. Zhang, Y. W., Jones, T. L., Martin, S. E., Caplen, N. J., and Pommier, Y. (2009) Implication of checkpoint kinase-dependent up-regulation of ribonucleotide reductase R2 in DNA damage response. *J. Biol. Chem.* **284**, 18085–18095
62. Conroy, T., Hammel, P., Hebbar, M., Ben Abdelghani, M., Wei, A. C., Raoul, J. L., *et al*. (2018) FOLFIRINOX or gemcitabine as adjuvant therapy for pancreatic cancer. *N. Engl. J. Med.* **379**, 2395–2406
63. Amrutkar, M., and Gladhaug, I. P. (2017) Pancreatic cancer chemoresistance to gemcitabine. *Cancers (Basel)* **9**, 157
64. Geller, L. T., Barzily-Rokni, M., Danino, T., Jonas, O. H., Shental, N., Nejman, D., *et al*. (2017) Potential role of intratumor bacteria in mediating tumor resistance to the chemotherapeutic drug gemcitabine. *Science* **357**, 1156–1160
65. Bepler, G., Kusmartseva, I., Sharma, S., Gautam, A., Cantor, A., Sharma, A., *et al*. (2006) RRM1 modulated *in vitro* and *in vivo* efficacy of gemcitabine and platinum in non-small-cell lung cancer. *J. Clin. Oncol.* **24**, 4731–4737
66. Masumori, N., Kunishima, Y., Hirobe, M., Takeuchi, M., Takayanagi, A., Tsukamoto, T., *et al*. (2008) Measurement of plasma concentration of gemcitabine and its metabolite dFdU in hemodialysis patients with advanced urothelial cancer. *Jpn. J. Clin. Oncol.* **38**, 182–185
67. Kim, M. P., and Gallick, G. E. (2008) Gemcitabine resistance in pancreatic cancer: picking the key players. *Clin. Cancer Res.* **14**, 1284–1285
68. Yang, M. C., Wang, H. C., Hou, Y. C., Tung, H. L., Chiu, T. J., and Shan, Y. S. (2015) Blockade of autophagy reduces pancreatic cancer stem cell activity and potentiates the tumoricidal effect of gemcitabine. *Mol. Cancer* **14**, 179
69. Kopper, F., Binkowski, A. M., Bierwirth, C., and Dobbelstein, M. (2014) The MAPK-activated protein kinase 2 mediates gemcitabine sensitivity in pancreatic cancer cells. *Cell Cycle* **13**, 884–889
70. Zheng, C., Jiao, X., Jiang, Y., and Sun, S. (2013) ERK1/2 activity contributes to gemcitabine resistance in pancreatic cancer cells. *J. Int. Med. Res.* **41**, 300–306
71. Wang, J., Lohman, G. J., and Stubbe, J. (2007) Enhanced subunit interactions with gemcitabine-5'-diphosphate inhibit ribonucleotide reductases. *Proc. Natl. Acad. Sci. U. S. A.* **104**, 14324–14329
72. Bergman, A. M., Pinedo, H. M., and Peters, G. J. (2002) Determinants of resistance to 2',2'-difluorodeoxycytidine (gemcitabine). *Drug Resist. Updat.* **5**, 19–33
73. Mencia, N., Selga, E., Rico, I., de Almagro, M. C., Villalobos, X., Ramirez, S., *et al*. (2010) Overexpression of S100A4 in human cancer cell lines resistant to methotrexate. *BMC Cancer* **10**, 250
74. Yuan, T. M., Liang, R. Y., Hsiao, N. W., and Chuang, S. M. (2014) The S100A4 D10V polymorphism is related to cell migration ability but not drug resistance in gastric cancer cells. *Oncol. Rep.* **32**, 2307–2318
75. Tabata, T., Tsukamoto, N., Fooladi, A. A., Yamanaka, S., Furukawa, T., Ishida, M., *et al*. (2009) RNA interference targeting against S100A4 suppresses cell growth and motility and induces apoptosis in human pancreatic cancer cells. *Biochem. Biophys. Res. Commun.* **390**, 475–480
76. Tsukamoto, N., Egawa, S., Akada, M., Abe, K., Saiki, Y., Kaneko, N., *et al*. (2013) The expression of S100A4 in human pancreatic cancer is associated with invasion. *Pancreas* **42**, 1027–1033
77. Kim, S. O., Jeong, J. Y., Kim, M. R., Cho, H. J., Ju, J. Y., Kwon, Y. S., *et al*. (2008) Efficacy of gemcitabine in patients with non-small cell lung cancer according to promoter polymorphisms of the ribonucleotide reductase M1 gene. *Clin. Cancer Res.* **14**, 3083–3088
78. Mlak, R., Krawczyk, P., Ramlau, R., Kalinka-Warzocha, E., Wasylecka-Morawiec, M., Wojas-Krawczyk, K., *et al*. (2013) Predictive value of ERCC1 and RRM1 gene single-nucleotide polymorphisms for first-line platinum- and gemcitabine-based chemotherapy in non-small cell lung cancer patients. *Oncol. Rep.* **30**, 2385–2398
79. Hagmann, W., Jesnowski, R., and Lohr, J. M. (2010) Interdependence of gemcitabine treatment, transporter expression, and resistance in human pancreatic carcinoma cells. *Neoplasia* **12**, 740–747
80. Giovannetti, E., Del Tacca, M., Mey, V., Funel, N., Nannizzi, S., Ricci, S., *et al*. (2006) Transcription analysis of human equilibrative nucleoside transporter-1 predicts survival in pancreas cancer patients treated with gemcitabine. *Cancer Res.* **66**, 3928–3935
81. Achiwa, H., Oguri, T., Sato, S., Maeda, H., Niimi, T., and Ueda, R. (2004) Determinants of sensitivity and resistance to gemcitabine: the roles of human equilibrative nucleoside transporter 1 and deoxycytidine kinase in non-small cell lung cancer. *Cancer Sci.* **95**, 753–757
82. Le Large, T. Y. S., El Hassouni, B., Funel, N., Kok, B., Piersma, S. R., Pham, T. V., *et al*. (2019) Proteomic analysis of gemcitabine-resistant pancreatic cancer cells reveals that microtubule-associated protein 2 upregulation associates with taxane treatment. *Ther. Adv. Med. Oncol.* **11**. 1758835919841233

83. Yang, X. L., Lin, F. J., Guo, Y. J., Shao, Z. M., and Ou, Z. L. (2014) Gemcitabine resistance in breast cancer cells regulated by PI3K/AKT-mediated cellular proliferation exerts negative feedback via the MEK/MAPK and mTOR pathways. *Onco. Targets Ther.* **7**, 1033–1042
84. Kao, Y. T., Hsu, W. C., Hu, H. T., Hsu, S. H., Lin, C. S., Chiu, C. C., *et al*. (2014) Involvement of p38 mitogen-activated protein kinase in acquired gemcitabine-resistant human urothelial carcinoma sublines. *Kaohsiung J. Med. Sci.* **30**, 323–330
85. Shimizu, K., Nishiyama, T., and Hori, Y. (2017) Gemcitabine enhances Kras-MEK-induced matrix metalloproteinase-10 expression via histone acetylation in gemcitabine-resistant pancreatic tumor-initiating cells. *Pancreas* **46**, 268–275
86. Sadygov, R. G., Maroto, F. M., and Huhmer, A. F. (2006) ChromAlign: a two-step algorithmic procedure for time alignment of three-dimensional LC-MS chromatographic surfaces. *Anal. Chem.* **78**, 8207–8217
87. Xiang, Y., Liu, Y., Yang, Y., Hu, H., Hu, P., Ren, H., *et al*. (2015) A secretomic study on human hepatocellular carcinoma multiple drug-resistant cell lines. *Oncol. Rep.* **34**, 1249–1260
88. Nguyen, J. Q., and Irby, R. B. (2017) TRIM21 is a novel regulator of Par-4 in colon and pancreatic cancer cells. *Cancer Biol. Ther.* **18**, 16–25
89. Mooney, S. M., Rajagopalan, K., Williams, B. H., Zeng, Y., Christudass, C. S., Li, Y., *et al*. (2011) Creatine kinase brain overexpression protects colorectal cells from various metabolic and non-metabolic stresses. *J. Cell Biochem.* **112**, 1066–1075
90. Beaujouin, M., and Liaudet-Coopman, E. (2008) Cathepsin D overexpressed by cancer cells can enhance apoptosis-dependent chemosensitivity independently of its catalytic activity. *Adv. Exp. Med. Biol.* **617**, 453–461
91. Sagulenko, V., Muth, D., Sagulenko, E., Paffhausen, T., Schwab, M., and Westermann, F. (2008) Cathepsin D protects human neuroblastoma cells from doxorubicin-induced cell death. *Carcinogenesis* **29**, 1869–1877
92. Carew, J. S., Espitia, C. M., Esquivel, J. A., 2nd, Mahalingam, D., Kelly, K. R., Reddy, G., *et al*. (2011) Lucanthone is a novel inhibitor of autophagy that induces cathepsin D-mediated apoptosis. *J. Biol. Chem.* **286**, 6602–6613
93. Zhang, Z., Liu, Z., Chen, J., Yi, J., Cheng, J., Dun, W., *et al*. (2018) Resveratrol induces autophagic apoptosis via the lysosomal cathepsin D pathway in human drug-resistant K562/ADM leukemia cells. *Exp. Ther. Med.* **15**, 3012–3019
94. Sun, X., Wei, Q., Cheng, J., Bian, Y., Tian, C., Hu, Y., *et al*. (2017) Enhanced Stim1 expression is associated with acquired chemo-resistance of cisplatin in osteosarcoma cells. *Hum. Cell.* **30**, 216–225
95. Kondratska, K., Kondratskyi, A., Yassine, M., Lemonnier, L., Lepage, G., Morabito, A., *et al*. (2014) Orai1 and STIM1 mediate SOCE and contribute to apoptotic resistance of pancreatic adenocarcinoma. *Biochim. Biophys. Acta.* **1843**, 2263–2269
96. Moinuddin, F. M., Shinsato, Y., Komatsu, M., Mitsuo, R., Minami, K., Yamamoto, M., *et al*. (2016) ATP7B expression confers multidrug resistance through drug sequestration. *Oncotarget* **7**, 22779–22790
97. Li, Y. Q., Yin, J. Y., Liu, Z. Q., and Li, X. P. (2018) Copper efflux transporters ATP7A and ATP7B: Novel biomarkers for platinum drug resistance and targets for therapy. *IUBMB Life* **70**, 183–191
98. Owatari, S., Akune, S., Komatsu, M., Ikeda, R., Firth, S. D., Che, X. F., *et al*. (2007) Copper-transporting P-type ATPase, ATP7A, confers multidrug resistance and its expression is related to resistance to SN-38 in clinical colon cancer. *Cancer Res.* **67**, 4860–4868
99. Samimi, G., Varki, N. M., Wilczynski, S., Safaei, R., Alberts, D. S., and Howell, S. B. (2003) Increase in expression of the copper transporter ATP7A during platinum drug-based treatment is associated with poor survival in ovarian cancer patients. *Clin. Cancer Res.* **9**, 5853–5859
100. Li, Z. H., Zheng, R., Chen, J. T., Jia, J., and Qiu, M. (2016) The role of copper transporter ATP7A in platinum-resistance of esophageal squamous cell cancer (ESCC). *J. Cancer* **7**, 2085–2092
101. Moinuddin, F. M., Hirano, H., Shinsato, Y., Higa, N., Arita, K., and Furukawa, T. (2017) ATP7B expression in human glioblastoma is related to temozolomide resistance. *Oncol. Lett.* **14**, 7777–7782
102. Schmid, S. C., Schuster, T., Horn, T., Gschwend, J., Treiber, U., and Weirich, G. (2013) Utility of ATP7B in prediction of response to platinum-based chemotherapy in urothelial bladder cancer. *Anticancer Res.* **33**, 3731–3737
103. Xu, X., Chai, S., Wang, P., Zhang, C., Yang, Y., Yang, Y., *et al*. (2015) Aldehyde dehydrogenases and cancer stem cells. *Cancer Lett.* **369**, 50–57
104. Januchowski, R., Wojtowicz, K., and Zabel, M. (2013) The role of aldehyde dehydrogenase (ALDH) in cancer drug resistance. *Biomed. Pharmacother.* **67**, 669–680
105. Wang, N. N., Wang, L. H., Li, Y., Fu, S. Y., Xue, X., Jia, L. N., *et al*. (2018) Targeting ALDH2 with disulfiram/copper reverses the resistance of cancer cells to microtubule inhibitors. *Exp. Cell Res.* **362**, 72–82
106. Raha, D., Wilson, T. R., Peng, J., Peterson, D., Yue, P., Evangelista, M., *et al*. (2014) The cancer stem cell marker aldehyde dehydrogenase is required to maintain a drug-tolerant tumor cell subpopulation. *Cancer Res.* **74**, 3579–3590
107. Abedini, M. R., Wang, P. W., Huang, Y. F., Cao, M., Chou, C. Y., Shieh, D. B., *et al*. (2014) Cell fate regulation by gelsolin in human gynecologic cancers. *Proc. Natl. Acad. Sci. U. S. A.* **111**, 14442–14447
108. Wang, P. W., Abedini, M. R., Yang, L. X., Ding, A. A., Figeys, D., Chang, J. Y., *et al*. (2014) Gelsolin regulates cisplatin sensitivity in human head-and-neck cancer. *Int. J. Cancer* **135**, 2760–2769
109. Boyer, J., Allen, W. L., McLean, E. G., Wilson, P. M., McCulla, A., Moore, S., *et al*. (2006) Pharmacogenomic identification of novel determinants of response to chemotherapy in colon cancer. *Cancer Res.* **66**, 2765–2777
110. Stevenson, L., Allen, W. L., Proutski, I., Stewart, G., Johnston, L., McCloskey, K., *et al*. (2011) Calbindin 2 (CALB2) regulates 5-fluorouracil sensitivity in colorectal cancer by modulating the intrinsic apoptotic pathway. *PLoS One* **6**, e20276
111. Jinawath, N., Vasoontara, C., Jinawath, A., Fang, X., Zhao, K., Yap, K. L., *et al*. (2010) Oncoproteomic analysis reveals co-upregulation of RELA and STAT5 in carboplatin resistant ovarian carcinoma. *PLoS One* **5**, e11198